Meteoritics & Planetary Science 39, Nr 6, 899–930 (2004)
Abstract available online at http://meteoritics.org

First petrographic results on impactites from the Yaxcopoil-1 borehole, Chicxulub structure, Mexico

Martin G. TUCHSCHERER,[1] W. Uwe REIMOLD,[1*] Christian KOEBERL,[2]
Roger L. GIBSON,[1] and Deon de BRUIN[3]

[1]Impact Cratering Research Group, School of Geosciences, University of the Witwatersrand, Private Bag 3, P.O. Wits, 2050 Johannesburg, South Africa
[2]Department of Geological Sciences, University of Vienna, Althanstrasse 14, A-1090 Vienna, Austria
[3]Council for Geosciences, Private Bag X112, 0001 Pretoria, South Africa
[*]Corresponding author. E-mail: reimoldw@geosciences.wits.ac.za

(Received 1 September 2003; revision accepted 14 April 2004)

Abstract–The ICDP Yaxcopoil-1 (Yax-1) borehole located 60 km south-southwest of the center of the Chicxulub impact structure intercepted an interval of allogenic impactites (depth of 795–895 m). Petrographic analysis of these impactites allows them to be differentiated into five units based on their textural and modal variations. Unit 1 (795–922 m) comprises an apparently reworked, poorly sorted and graded, fine-grained, clast-supported, melt fragment-bearing suevitic breccia. The interstitial material, similar to units 2 and 3, is permeated by numerous carbonate veinlets. Units 2 (823–846 m) and 3 (846–861 m) are groundmass-supported breccias that comprise green to variegated angular and fluidal melt particles. The groundmass of units 2 and 3 comprises predominantly fine-grained calcite, altered alkali element-, Ca-, and Si-rich cement, as well as occasional lithic fragments. Unit 4 (861–885 m) represents a massive, variably devitrified, and brecciated impact melt rock. The lowermost unit, unit 5 (885–895 m), comprises highly variable proportions of melt rock particles (MRP) and lithic fragments in a fine-grained, carbonate-dominated groundmass. This groundmass could represent either a secondary hydrothermal phase or a carbonate melt phase, or both. Units 1 and 5 contain well-preserved foraminifera fossils and a significantly higher proportion of carbonate clasts than the other units. All units show diagnostic shock deformation features in quartz and feldspar clasts.

Our observations reveal that most felsic and all mafic MRP are altered. They register extensive K-metasomatism. In terms of emplacement, we suggest that units 1 to 3 represent fallout suevite from a collapsing impact plume, whereby unit 1 was subsequently reworked by resurging water. Unit 4 represents a coherent impact melt body, the formation of which involved a significant proportion of crystalline basement. Unit 5 is believed to represent an initial ejecta/ground-surge deposit.

INTRODUCTION

Since its discovery (Penfield and Camargo 1981; Hildebrand et al. 1991), the Chicxulub impact structure has been widely accepted as the "smoking gun" for the catastrophic impact event associated with the 65 Ma Cretaceous-Tertiary (K/T) boundary. Recent publications that question this association (Keller et al. 2003a, 2004) are based on very limited data that are quite questionable. Crucial evidence in support of a collision with an extraterrestrial projectile at that time includes the widespread deposition of glass spherules around the Caribbean and beyond (e.g., Sigurdsson et al. 1991; Smit et al. 1992; Premo and Izett 1992; Koeberl and Sigurdsson 1992; Koeberl 1993; Oskarsson et al. 1996; Chaussidon et al. 1996; Hough et al. 1998; Smit 1999), the global distribution of shock metamorphic quartz (Bohor 1990; Owen et al. 1990; Alvarez et al. 1995; Bostwick and Kyte 1996; Goto et al. 2002), anomalous PGE concentrations with chondritic character (Alvarez et al. 1980; Kyte et al. 1980; Smit and Hertogen 1980; Orth et al. 1981; Schmitz 1988; Evans et al. 1995), Ni-rich spinels (Cisowski 1990; Kyte and Bostwick 1995; Gayraud et al. 1996), the presence of fullerenes (Heymann et al. 1994, 1996; Buseck 2002), evidence for a global occurrence of wildfires (Argyle et al. 1986; Wolbach et al. 1985, 1990; Kring and Durda 2001), and nano- to micro-diamonds found worldwide in the K/T boundary clay layer (Gilmour et al. 1992; Hough et al. 1997). The major mass

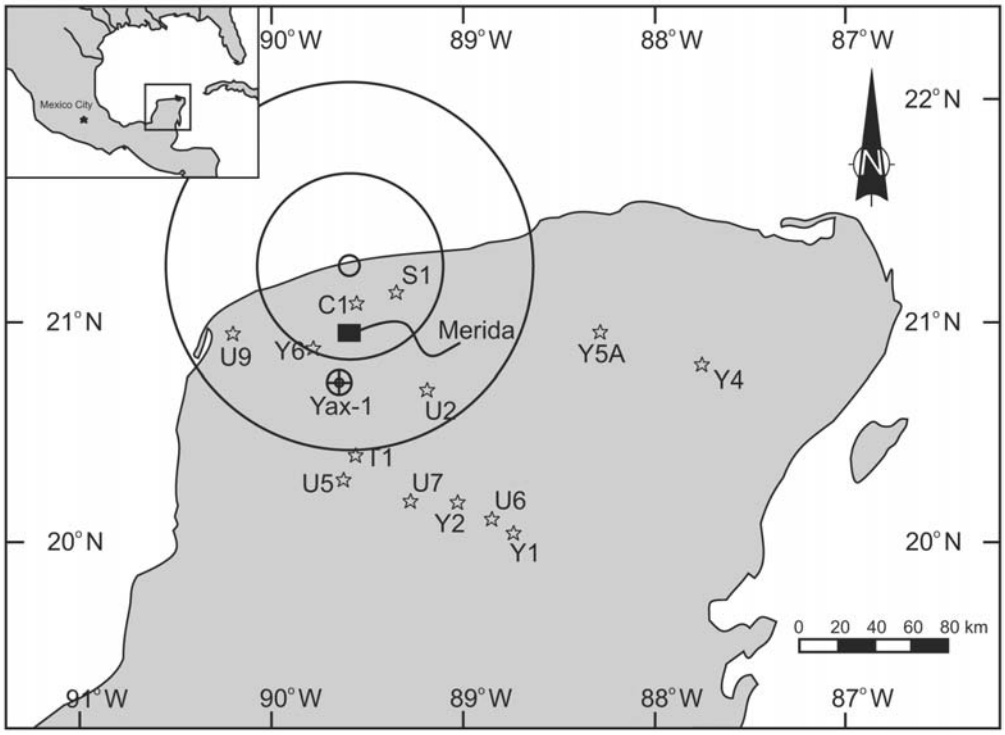

Fig. 1. The Chixculub meteorite impact site is located on the northwestern part of the Yucatán Peninsula of Mexico. The ICDP borehole is located ~60 km toward the south of the center of the structure. The circles shown here represent the extent of the postulated transient cavity at ~100 km (Morgan et al. 2002) and the crater diameter at ~195 km postulated from the position of the outermost, most significant inward-facing scarp (Morgan et al. 2002). Also shown are all nearby diamond drill hole localities (borehole localities from Persaud and Sharpton [1998] and Sharpton et al. [1999]).

extinction event at the K/T boundary has been widely linked to this cosmic catastrophe (e.g., Alvarez et al. 1980; Wolbach et al. 1985; Pope et al. 1994; and papers in Sharpton and Ward 1990; Ryder et al. 1996; and Koeberl and MacLeod 2003).

Impact melt rock and breccia samples provided the confirmation of the impact origin of the Chicxulub structure (Hildebrand et al. 1991; Kring and Boynton 1992; Swisher et al. 1992; Sharpton et al. 1992; Koeberl 1993; Blum et al. 1993; Schuraytz et al. 1994; Kettrup et al. 2000; Claeys et al. 2003). Some of the earlier findings placed constraints on the impact melt crystallization age and, thus, the age of the impact, its link to the K/T boundary mass extinction, and the geochemical characteristics and isotopic signature of the melt. These observations, however, have resolved neither the extent of melting by the Chicxulub impact event nor the extent of target rock mixing in the formation of the melt.

Because no other well-preserved impact structure of Chicxulub's size (~195 km in diameter; Morgan et al. 2002) is accessible for detailed analysis, the crater was re-drilled between December 2001 and February 2002 by the International Continental Scientific Drilling Program (ICDP; Dressler et al. 2003a, b). Chicxulub is the third largest impact structure currently identified on Earth (Grieve and Therriault 2001; Whitehead 2004) and the only such large one that is almost preserved (but, unfortunately, not well-accessible). For this reason, scientific drilling of the crater is the prime tool to elucidate the internal structure and fill of such a large impact structure. The Yaxcopoil-1 (Yax-1) borehole was drilled ~60 km from the center of the impact structure (Fig. 1) in anticipation of intersecting a thick and complete impactite sequence, as interpreted from geophysical data (e.g., Sharpton et al. 1996, their Fig. 5; Morgan et al. 2000, their Figs. 3 and 4) and suggested by the stratigraphy of neighboring earlier drill cores (Fig. 2). A complete section of impactite was desirable for its potential to contribute to solving important issues such as the total melt volume, mixing of target rocks, distribution and origin of shocked material, lateral distribution of ejecta, and fate of the meteoritic projectile.

However, the Yax-1 borehole intercepted only 100 m of impactites, probably because no seismic data existed for the borehole location. Here, we report our first results of a detailed petrographic investigation of this interval, including a detailed description of the various units, modal analyses, cathodoluminescence, scanning electron microscopic (SEM), electron microprobe (EMP), and X-ray diffraction (XRD) results. The objectives of this work are to provide petrographic constraints for the stratigraphic subdivision of various impactite units and their formation, constrain melt compositions, investigate primary versus secondary mineralogical features, characterize the lithic and mineral clast content in the impactites with a view to contributing to

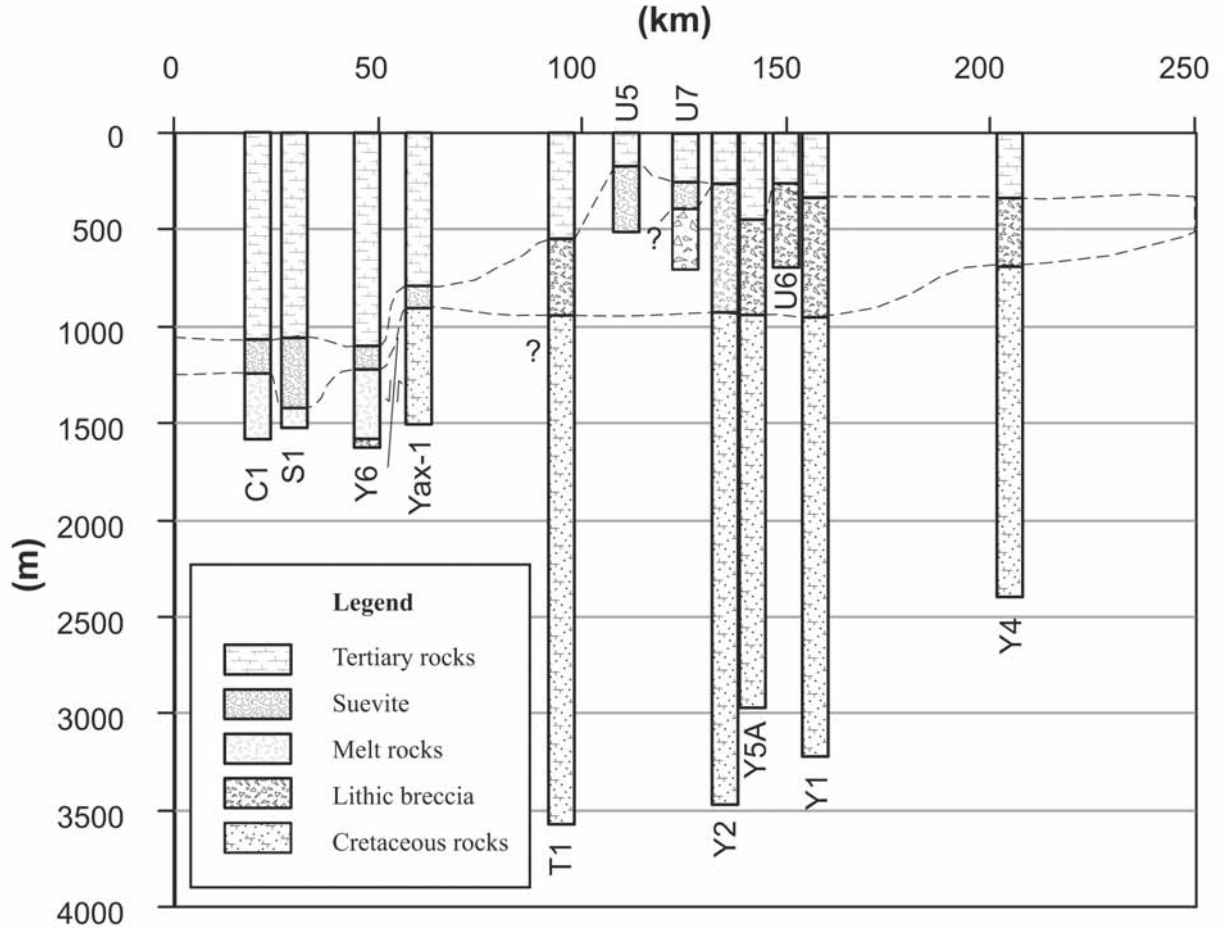

Fig. 2. Projected vertical cross section through the Chicxulub impact structure (0 km = crater center) with all published exploratory and scientific boreholes, as compiled by Stöffler et al. (2003b). Note that the Yax-1 borehole overlies a region of faulted and displaced Cretaceous rocks similar to the T1 borehole between 900 and 1500 m (Ward et al. 1995). It can be seen that the C1, S1, and Y6 boreholes were all drilled into a comparatively thicker sequence of Tertiary rocks, covering the infilled impact basin.

the understanding of the Chicxulub target composition, determine the nature of shock metamorphic effects in the clasts and their distribution over the stratigraphic section, and to integrate these results in an attempt to contribute to an emplacement model for this sequence.

PREVIOUS DRILLING OF CHICXULUB

As seen in Fig. 1, 14 boreholes have been drilled to date in the area of the Chicxulub structure and its immediate vicinity. Most cores (C1, S1, Y1, Y2, Y4, Y5A, Y6, T1; Fig. 1) were recovered by the Mexican national oil company PEMEX during hydrocarbon exploration in the late 1960s and 1970s (Hildebrand et al. 1991). The stratigraphies of these boreholes are compared in Fig. 2. After Chicxulub had been established as an impact structure (Hildebrand et al. 1991), additional drilling was undertaken by the Universidad Nacional Autonoma de Mexico (UNAM; boreholes 2, 5–7, 9). Although drilling was extensive, only few scientific publications on the petrology and the chemistry of impactites have been published to date (Hildebrand et al. 1991; Kring and Boynton 1992; Swisher et al. 1992; Sharpton et al. 1992; Koeberl 1993; Blum et al. 1993; Schuraytz et al. 1994; Meyerhoff et al. 1994; Ward et al. 1995; Warren et al. 1996; Urrutia-Fucugauchi et al. 1996; Kettrup et al. 2000; Claeys et al. 2003). Impact melt samples from the C1 and Y6 boreholes were described as having an andesitic to dacitic composition (Hildebrand et al. 1991; Kring and Boynton 1992; Sharpton et al. 1992; Warren et al. 1996). The Y6 samples were observed to be richer in platform-sedimentary clasts than the C1 samples (e.g., Schuraytz et al. 1994; Claeys et al. 2003). Borehole Y6 is located in the impact basin (the so-called moat) around the central peak ring. The T1 borehole is located just outside the crater rim (assuming a 195 km-wide crater; Morgan et al. 1997). Farther out from the center of the crater, samples from the UNAM 5, 7, and 6 boreholes were observed to contain progressively lower proportions of siliceous basement inclusions and an increasing sedimentary component (Urrutia-Fucugauchi et al. 1996; Sharpton et al. 1999).

Kring and Boynton (1992) showed that, compositionally, these melt rocks do not follow traditional calc-alkaline and tholeiitic igneous trends and demonstrated—in support of an impact origin—that Haitian impact melt lay on a similar mixing line as that established for Chicxulub impactites. Kring and Boynton (1992) indicated that the andesitic melt composition could be modeled as a mixture of upper sedimentary and crystalline basement rocks known to occur in the Yucatán crust, i.e., 12% (by volume) Y6-N17 groundmass, 72% mica schist, 4% sandstone, 2% dolomite, and 10% limestone/anhydrite. Sharpton et al. (1992) also showed that some of the the Y6 and C1 melt rocks contained unusually high abundances of iridium, the highest values being 2.5 ± 0.5 and 13.5 ± 0.9 ppb, indicating the presence of an extraterrestrial component, as also established for the K/T boundary layer at numerous locations (e.g., Alvarez et al. 1980). This was confirmed for C1 melt rocks by Koeberl et al. (1994) from osmium isotopic studies. Radiometric dating by Sharpton et al. (1992) of the Y6 and C1 melt rocks, with the ^{40}Ar-^{39}Ar technique, produced a crystallization age of 65.2 ± 0.4 Ma, similar to the results of Swisher et al. (1992). Schuraytz et al. (1994) suggested that Y6 and C1 crystalline impact melt rocks had undergone slow cooling and, thus, might be worth investigating for potential Sudbury-style mineralization. They also proposed that C1 or C3 carbonaceous chondrite meteorites could represent the type of projectile responsible for the formation of the Chicxulub crater, as the impactites contained rare but characteristic high-iridium particles only found in such meteorites. Warren et al. (1996) concluded that the clast content of impact melt rock from the C1 and Y6 drill cores was negatively correlated with matrix grain size, as also known from other impact structures. They proposed that the incorporation of cold inclusions into the impact melt acted as a heat sink, providing a quenching effect. Further insight into the subsurface stratigraphy of the Yucatán platform was given by Ward et al. (1995) through a compilation of logs from boreholes T1, Y2, Y1, Y6, C1, Y5, and Y4 (compare with Fig. 2). They emphasized that the basement was intersected at 2418 m and 3203 m in wells Y4 and Y1, respectively, and that it comprised a Paleozoic metamorphic terrain of Pan-African age (~545 Ma; Krogh et al. 1993; Kamo et al. 1995). Ward et al. (1995) postulated that the pre-impact sedimentary rock stratigraphy comprised 35 to 40 vol% dolomite, 25 to 30 vol% limestone, 25 to 30 vol% anhydrite, and 3 to 4 vol% sandstone and shale.

Petrographic and geochemical results from Chicxulub melt rocks (drill cores Y6 and C1) were recently reported by Kettrup et al. (2000, 2003) and Claeys et al. (2003). They indicated that the Chicxulub melt rocks are more heterogeneous than previously thought. Kettrup et al. (2000) concluded that a mafic component was required to model the variation between C1 melt rock and Haitian impact glasses. These authors also determined that the melt rocks and ejecta deposits had different isotopic and major element characteristics and, thus, indirectly revealed the complex geological character of the Yucatán crust. Kettrup et al. (2003) suggested that the Chicxulub impact may have sampled Gondwanan and Laurentian crust.

Claeys et al. (2003) recognized three subdivisions in the impactites of the Y6 borehole: i) an upper, fine-grained, carbonate-rich, fossil-bearing suevite; ii) a middle, relatively coarser-grained, suevite rich in altered silicate melt particles and silicate basement clasts; and iii) a lower, so called "thermometamorphic" suevite rich in melt fragments, large evaporite clasts, and shocked basement clasts. Thermal metamorphism of this latter unit, i.e., recrystallization of its groundmass, was thought by these authors to have been induced by an underlying, now crystalline, impact melt layer. Claeys et al. (2003) proposed that the upper suevite represented either a late fall-back deposit or an interval that was reworked by seawater resurging into the impact basin; the middle suevite represented a typical suevite deposit that originated as fall-back out of a collapsing ejecta plume; and the lower unit represented either an early ejecta/fall-back deposit or material that was deposited on the outermost flank of the collapsed transient cavity by inward movement of material during the modification stage of cratering.

The currently available data indicate that the Yucatán crust represents a much more varied geological terrain than previously thought. Inclusions observed within retrieved cores mostly originate from the crystalline basement and include granite, schist, gneiss, and amphibolite, besides a sedimentary, carbonate- and anhydrite-dominated, component. The crystalline lithologies represent a metamorphic terrane that is related to the Grenvillian orogeny (Kettrup et al. 2003) and that also involves crust that was recycled during Pan-African times.

THE YAXCOPOIL-1 DRILL CORE

Yaxcopoil-1 is located ~60 km from the center of the Chicxulub structure (Fig.1). It extends to a final depth of 1511 m (Fig. 2). The drill site was chosen to better elucidate the composition of the structure in a gap between a string of earlier boreholes (Sharpton 2000; our Fig. 2) and because a thick impactite intersection was expected. Prior to drilling, detailed geophysical analysis was carried out to constrain the sub-surface structure and geology. As shown by Sharpton et al. (1996, their Fig. 5), extensive breccia deposits and melt rocks were expected to be intersected at the Yax-1 site, at least comparable to those in the Y6 and T1 boreholes, where 490 m of suevite and melt rocks and 930 m of "Bunte breccia"-like deposits had been intersected, respectively. Geophysical data (gravity, Sharpton et al. 1993; seismics, Morgan et al. 1997, 2000, 2002) predicted that the site, located in an annular trough around the peak ring structure, was favorable for preservation of a thick breccia deposit. From the seismic data, it was also determined that the Cretaceous rocks at the Yax-1

site seemingly were part of disturbed, slumped blocks that occurred between 40 and 75 km from the crater center. Based on the interpretation of geophysical information (Morgan et al. 2002), the drilling site corresponded to a point ~37.5 km inward from the crater rim.

The Yax-1 borehole intersected 795 m of Tertiary rocks (mostly interlayered carbonaceous siltstones and calcarenites), 100 m of suevitic breccia and melt rock, and 615 m of presumably displaced Cretaceous rocks (comprising interlayered calcarenite, dolomite, and anhydrite, with minor siltstones and conglomerates) (Dressler et al. 2003a, b). The field log for the drill-core and the terminology developed by Dressler (2003a, b) provide a stratigraphic basis for all ongoing investigations (Table 1). The focus of our work, the impactite sequence, was initially differentiated into six stratigraphic units based on macroscopic core logging observations (color, grain size, fabric, and texture); most groups working on this drill core have accepted this general stratigraphy, but as we will discuss in detail below, we favor a five-fold division.

Borehole Stratigraphy

The borehole stratigraphy can be summarized as follows, after Dressler et al. (2003a): upper Tertiary rocks were intersected from a depth of 404 m (beginning of continuous coring) to 795 m. This interval comprises a foraminifera-rich, rhythmic laminated, hemipelagic sequence of anoxic limestones that alternate with bioturbated marls (Dressler et al. 2003a). Below a depth of 600 m, several conglomeratic mass flows are intercalated with hemipelagic sediments (calcarenite, calcareous siltstone, and minor chert). Between 795 and 895 m, a 100 m-thick impactite sequence was drilled (see our detailed descriptions for units 1 to 5 below). Below this depth, sedimentary platform rocks comprise poorly fossiliferous limestone, dolomite, and anhydrite, of which the latter makes up 27.4% (Dressler et al. 2003a). Several breccia zones were intersected in these Cretaceous rocks: melt-bearing breccias at ~909–910, 916, 1348 m; lithic breccias at 1314–1316, 1341, 1398–1399 m; black oil-bearing shear zones at 1350, 1369, 1372, 1382, 1394, 1397, 1399, 1420 m; and several wide, brittle deformation zones between 1310–1400 m and 1496–1510 m (Kenkmann et al. 2003).

Dressler (2003a, b) identified a number of key lithological criteria for each impactite unit (Table 1). Laminations, at the top, and clast size sorting are observed within his unit 1 (795–808 m). Unit 2 (808–823 m), in contrast, contains no lamination or clast-size sorting. Unit 3 (823–846 m) was defined by a distinct fine-grained, brown matrix—thought to be a melt matrix—that supports relatively fewer large melt and lithic fragments than observed in the upper units. Thus, unit 3 was termed a "chocolate-brown melt breccia" (Dressler et al. 2003a). Unit 4 (846–861 m) displays a very coarse and heterogeneous character that involves contorted, flow-structured, and welded melt fragments of various colors, from which this unit gained its working name "suevitic breccia, variegated, melt-rich." This unit has a gradational contact with unit 3. Unit 5 (861–885 m) displays an abrupt upper contact. It is characterized by flow-structured green melt fragments that locally fit together like the pieces of a jigsaw puzzle and was, thus, named "green, monomict, autogene melt breccia" by Dressler et al. (2003a). The green melt fragments are, in places, supported by a fine-grained carbonate matrix that contains a high proportion of originally mostly molten basement rock clasts. The lowermost impactite unit (unit 6, 885–895 m) follows with a gradational upper contact and displays an increase in size, abundance, and diversity of target rock fragments. Melt fragments display green to tan and light gray colors. The carbonate groundmass is light tan to light brown. The groundmass is locally flow-textured and contains very small target rock fragments and melt rock particles. This unit was, thus, named "variegated, polymict, allogenic, clast-rich melt breccia" (Dressler et al. 2003a).

PETROGRAPHIC RESULTS

Macroscopic Observations

Macroscopic observations were made on the Yax-1 core samples at the first ICDP sampling party at UNAM, Mexico City, in April 2002. In this section, a description of the impactites and some of the overlying reworked suevitic/carbonate material is presented. From top to bottom of the impactite interval, five units (Tables 1 and 2) are distinguished on the basis of melt rock content, melt fragment size, morphology, color, groundmass type, and lithic mineral clast content.

Top Reworked Suevitic and Sedimentary Rocks

The 50 cm interval above the upper impactite contact, between depths of 794.1 and 794.6 m, comprises a very fine-grained, medium-brown to light beige carbonate interval. Fine-scale cross bedding characterizes the overlying material. Also observed are 1 cm-thick, green, sedimentary lenses of reworked, altered, green melt particles. Rare, small, variegated and spotted drop-stones ~1 cm in size—possibly representing fragments of the underlying reworked suevite—were also noted. This interval grades over 5 cm into the underlying, massive suevitic rocks.

Unit 1

The uppermost impactite between 795 and 808 m depth comprises a heavily altered and reworked suevitic rock containing a large proportion of altered, green melt rock particles. The rock is largely particle-supported. Melt particles are sub-rounded, microcrystalline, and relatively well-sorted compared to the underlying units. The average fragment size is ~2 mm. This unit is extremely friable (poorly consolidated) and was, therefore, not diamond sawed for sampling. According to Dressler et al. (2003a), there is a sharp contact with the underlying package at ~808 m. The

Table 1. Comparison of Yax-1 impactite lithological units, as proposed by various research groups.

Units	Depth (m)	Dressler et al. 2003a, b	Stöffler et al. 2003a	Kring et al. 2003a	Tuchscherer et al. 2003 and this study
1	795–808	Redeposited suevite	Upper sorted suevite (USS)	Fine-grained reworked suevite (13 m)	Fining upwards, sorted, and reworked suevite
2	808–823	Suevite	Lower sorted suevite (LSS)	Matrix /clast supported suevite (15 m)	
3	823–846	Chocolate-brown melt breccia	Upper suevite (US)	Melt-rich breccia (23 m)	Suevite
4	846–861	Suevitic breccia, variegated, glass rich	Middle suevite (MS)	Melt-rich breccia agglomerate (15 m)	Variegated, melt rock fragment-rich suevite
5	861–885	Green, monomict, autogene melt breccia	Suevitic breccia with cataclastic melt rock (SB)	Coherent, massive, green impact melt unit (24 m)	Green impact melt, brecciated
6	885–895	Variegated, polymict, allogenic, clast melt breccia	Lower suevite (LS)	Brecciated, carbonate-charged, green melt unit (10 m)	Variegated, polymict, impact melt breccia or suevite

Table 2. Yax-1 impactite-lithological characteristics (this study).

Units	Depth (m)	Lithological characteristics
1	795–823	Fining upward, sorted, reworked, and clast-supported breccia deposit. Contains limestone and fossil fragments. Altered melt typically has greenish color.
2	823–846	A fine-grained, groundmass-supported breccia that contains green fluidal textured, angular and rounded melt rock fragments.
3	846–861	A fine-grained, groundmass-supported breccia that contains variegated, angular, and rounded melt rock fragments. Abundance of large brown melt rock masses increases with depth.
4	861–885	A massive but strongly brecciated green melt rock unit. Melt fragments display flow-textures.
5	885–895	A melt breccia comprising variegated altered melt rock fragments and polymict lithic/mineral clasts and foraminifera suspended in a fine-grained carbonate groundmass.

material between 808 and 823 m is distinctly more consolidated than the upper part of unit 1. Compared to the overlying segment, angular (shard-like) melt and lithic particles become progressively more inequigranular (less sorted), coarser (average ~8 mm, generally 2 cm), and angular with depth (Fig. 3a). Most melt particles are green, others are brown or dark gray. Recognizable lithic inclusions comprise primarily sedimentary clasts including limestone, dolomite, and siltstone but also a few small (<0.5 cm), mottled, pinkish-white granitic clasts.

Unit 2

The upper and lower contacts of this unit, at 823 and 846 m, respectively, are gradational, but relative to unit 3, unit 2 has a distinctive color, lithic fragment population and size, and melt particle size. Relative to the predominantly light olive-green unit 1, the groundmass in unit 2 is medium gray. This color only became apparent upon drying out of the core—immediately after extraction of the core, the groundmass was medium-brown. Clasts in this unit are highly inequigranular. This breccia carries a variety of angular melt rock fragments of shard-like appearance that, in part, show schlieren (fluidal texture; Fig. 3b). Dark gray and brown melt fragments are also observed. All melt fragments are suspended in a microcrystalline to cryptocrystalline groundmass (Fig. 3b). Melt fragments are generally larger in this unit—~2 cm on average but up to 9 cm in diameter—than in unit 1. Recognizable lithic inclusions are derived from limestone, siltstone, and granite.

Unit 3

Unit 3, between depths of 846 and 861 m, displays a gradational upper contact but a sharp lower contact. This material (Fig. 3c) consists of subrounded/subangular melt particles that locally display shard forms and a range of colors (brown, gray, and green) and commonly show distinct, beige reaction rims. The average fragment size is similar to that in unit 2, at 2 cm, but larger fragments occur in relatively greater abundance. The proportion of brown melt rock particles increases with depth (as discussed in detail below). Lithic fragments are rare and generally comprise small (5–10 mm), rounded limestone clasts, besides a few silicate (granite, schist) inclusions. Calcite veins permeate the groundmass and anastomose around melt shards.

Unit 4

Unit 4, from 861 to 885 m, is a massive green unit dominated by large, angular to subangular melt fragments (Fig. 3d). The shard-like melt fragments display internal fluidal textures, and the jigsaw-like arrangement of fragments indicates that this melt experienced in situ brecciation. The material interstitial to the shards is fine-grained, dark gray, and cannot be resolved in hand specimen.

Unit 5

The lowermost impactite unit, between 885 and 895 m, displays a locally variable population of lithic fragments and melt particles. A 34 cm-wide granitic clast was observed at a depth of 889.59 m. Other lithic fragments that can be

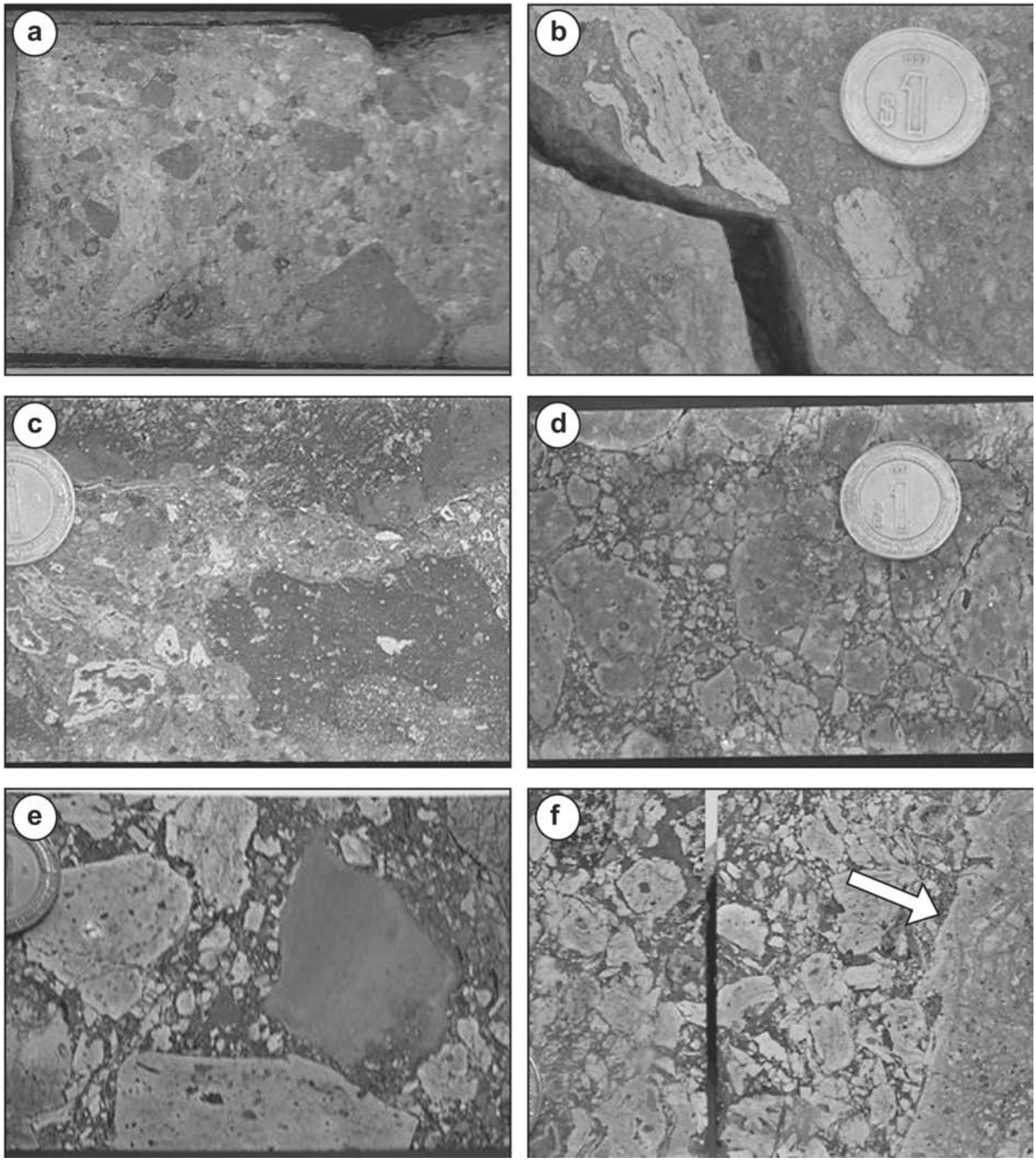

Fig. 3. Photographs of the various lithological units taken in the impactite interval of the Yax-1 borehole, core width = 6.35 cm, coin diameter = 2 cm: a) unit 1, reworked suevite, depth = 811.55 m; b) unit 2, un-reworked suevite, depth = 835.31 m; c) unit 3, variegated melt rock rich suevite, depth = 851.85 m; d) unit 4, brecciated green impact melt rock, depth = 862.81 m; e) unit 5, variegated polymictic impact melt breccia, depth = 889.88 m; f) unit 5, undulating contact between coarse- and a fine-grained breccia, image height = 6.2 cm, depth = 892.55 m. See text for detail.

recognized macroscopically represent dolomite and limestone. Sub-angular and relatively large (2–5 cm) melt particles, often with internal flow structures, are suspended within a fine-grained, carbonate-dominated groundmass (Fig. 3e). Sharp undulating contacts were also observed within the brecccia (Fig. 3f; at a depth of 892.55 m).

Micro-Analysis

In total, 52 polished thin sections of samples from the impactite interval were prepared for petrographic analysis. It is important to bear in mind the small sample size: only specimens between 8 to 16 cm^3 were provided. In the light of

lithic and melt fragment diversity, as well as the large variation of grain sizes observed, the representivity of our sample suite must be considered. In point counting analysis, 1000 counts were recorded per thin section, at 0.25 mm increments and 1 mm line spacing. Cathodoluminescence (CL) properties were observed using an Olympus BH-2 petrographic microscope connected to a cold-cathode CITL MK3a CL apparatus at 10 ± 2 kV and 300 ± 25 μA operating conditions, with the vacuum maintained at 0.3–0.7 mTorr. Backscattered electron imaging and energy-dispersive X-ray analysis were carried out, at 15–20 kV, 20 nA, and 39 to 15 mm working distances, with a JSM-840 scanning electron microscope (SEM) at the Electron Microscope Unit of the University of the Witwatersrand. Additional imaging was done at the Council for Geoscience, Pretoria, with a Leica 440 Stereoscan instrument with attached LINK OXFORD energy-dispersive X-ray analysis system at 20 kV, 2 nA, and a 25 mm working distance. Quantitative electron microprobe analyses were collected for the elements Si, Ti, Al, Cr, Fe, Mn, Mg, Ca, and Na in wavelength-dispersive mode on a JEOL 733 Superprobe at 15 kV, 20 nA, and a 39 mm working distance, also at the Council for Geoscience in Pretoria. Electron-beam widths ranged from 3 to 10 μm with peak count times of 10 sec and 5 sec each on symmetrical background positions. The standard K-H, a hornblende from Kakanui, New Zealand (USNM 143965; see Jarosewich et al. 1980), was used for SiO_2, Al_2O_3, FeO_{tot}, CaO, Na_2O, and K_2O analysis, synthetic rutile was used for TiO_2, natural rhodonite was used for MnO, and the chromite standard USNM 117075 was used for Cr_2O_3 standardization. Data reduction was done with the JEOL Fortran program (FZAFOC). X-ray diffraction analyses on bulk rock powders were carried out with the PW 1710 instrument at the X-ray analytical facility of the School of Geosciences at the University of the Witwatersrand.

Microscopic Observations

A summary of the key micro-petrographic observations made on samples of the various impactite units is given in this section.

Unit 1

Thin sections of unit 1 breccia reveal relatively small lithic clasts and melt fragments that commonly have shard-like forms. These particles range in size from 0.1 to 4 mm and have an estimated average size of 2 mm. The melt particles are primarily angular to subangular. They are self-supported. The fragments are surrounded primarily by an interstitial network of fine-grained carbonate veins and/or by a microcrystalline (<0.05 mm) groundmass containing small carbonate grains interspersed with a very fine-grained silicate cement (Fig. 4a), as also observed by Ames et al. (2003) and Kring et al. (2003a). The melt fragments are extensively altered; they are predominantly green but can also be grayish-brown or colorless. With increasing depth, the color of the altered melt fragments shifts from a dominant greenish-yellow to more yellowish-green hues. Microscopic perlitic fractures characterize the melt fragments, dividing the fragments into domains of typically <0.05 mm width. The samples also contain rare, very small, brown to dark gray, fluidal-structured, altered melt fragments, and even more rare, orange-red melt particles (Fig. 4b). An increasing abundance of large (5–15 mm), angular, fluidal-textured, dark gray and brown melt particles is noted with increasing depth. Lithic inclusions are rare and include, with decreasing relative abundance, limestone, dolomite, shale, quartzite, granite, and schist fragments. Mineral fragments are very rare and include, again in decreasing abundance, calcite, dolomite, quartz, and feldspar. The abundance of microscopic calcareous shells and foraminiferous limestone (Fig. 4c) is a key characteristic of unit 1 (compare Table 3). They are found within carbonate clasts or are freely suspended in the groundmass. Numerous melt fragments have small blebs of carbonate that represent either infilled vesicles or evidence of liquid immiscibility of a carbonate melt phase in silicate melts. Fine-grained (~1 mm) and relatively wide (2 mm) carbonate veins commonly cut through the fine-grained carbonate-rich groundmass and meander around lithic and melt fragments.

Samples from the section between 808 and 823 m and from close to the gradational contact with unit 2 contain more angular and vesiculated green melt fragments and rarer fluidal-structured shard-like melt fragments (size range 0.5–5 mm, average size 2.5 mm) than elsewhere in this unit. These fragments are also self-supported and are set in a vein network of very fine-grained (<0.05 mm) to, in patches, fine-grained (~0.5–1.0 mm), white to light gray interstitial carbonate. Small (~0.25 mm) lithic (quartzite/chert, limestone, dolomite) inclusions and large (up to 15 mm), brown or dark gray melt fragments are also present. Quartz grains are usually found with one set of planar deformation features (PDFs), sometimes with more, and may display an unusual, angular fracture pattern similar to the "cracked tile" texture known from cristobalite (Deer et al. 1996). Melt fragments can be disaggregated, brecciated, or shattered and are generally extensively altered. In this interval, larger melt particles with fewer perlitic fractures are found with increasing depth.

Unit 2

Melt fragments in this unit are angular to sub-rounded and locally display internal fluidal structures. Some melt fragments are vesiculated and display frothy (Fig. 5a) morphologies. The melt fragment size is one to two orders of magnitude larger than in unit 1, ranging from 0.5 to 6 mm (averaging at 4 mm). In contrast to the melt fragments of unit 1, melt fragments in unit 2 contain abundant microlites. The long axes of microlites are frequently aligned, indicating

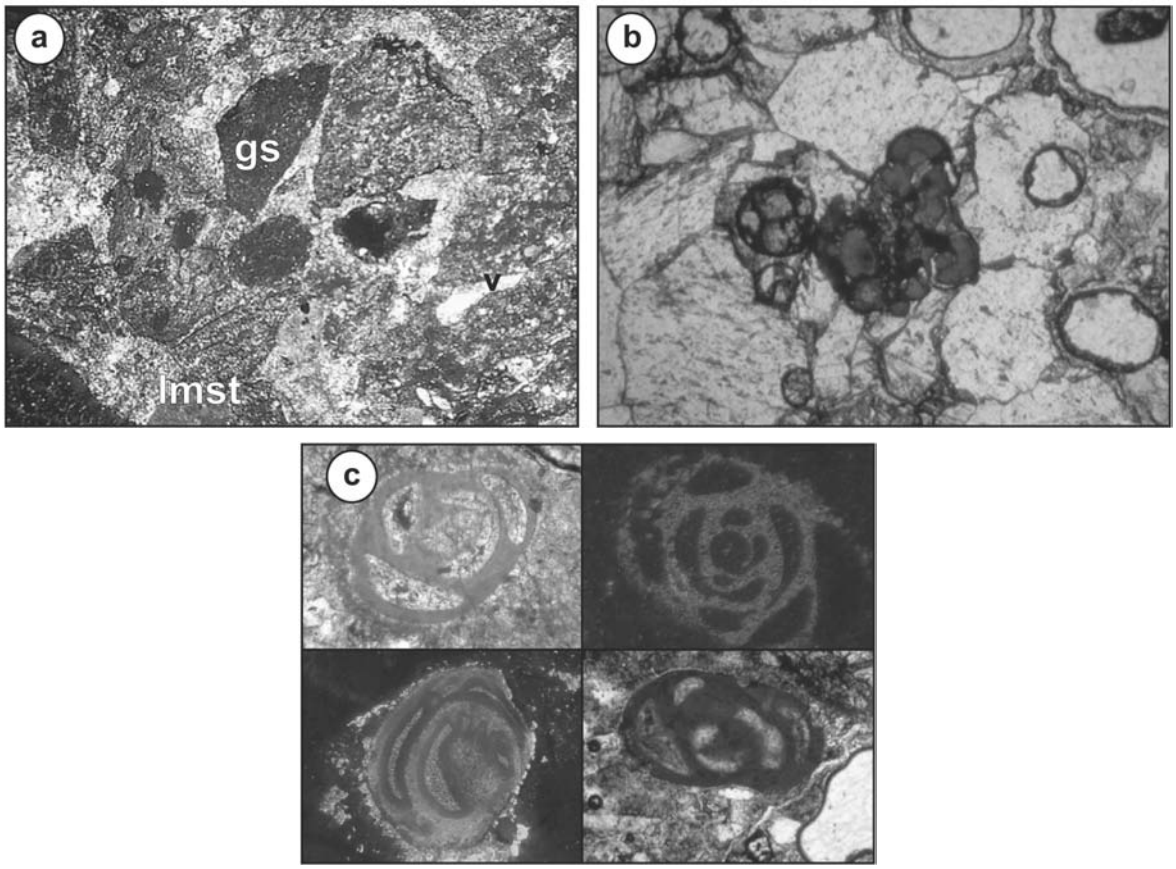

Fig. 4. Photomicrographs of unit 1: a) fragmental, angular to rounded, and vesiculated clast-supported glass shards (gs) set into a microcrystalline carbonate groundmass; note the limestone (lmst) fragment at the bottom of image; image width = 4 mm, cross polarized light (CPL), sample depth = 803.44 m; b) botryoidal red glassy bleb in a medium-grained calcite patch; image width = 1.5 mm, plane polarized light (PPL), sample depth = 809.70 m; c) various foraminifera fossils: top-right foraminifera width = 0.65 mm, cathodoluminescence image (CL), sample depth = 809.70 m; bottom-right foraminifera width = 2 mm, PPL, sample depth = 803.48 m; bottom-left foraminifera width = 2 mm, CL, sample depth = 809.70 m; top-left foraminifera width = 1.5 mm, PPL, sample depth = 803.48 m.

flow within the melts at the time of crystallization (Fig. 5b and 5c). Most of these fragments are groundmass-supported. As seen in Fig. 5a, vesicles can be filled with calcite, whereas others are filled with the very fine-grained groundmass material. Locally, carbonate blebs with ovoid shapes are observed in melt fragments; they may be extended parallel to the prevailing microlite orientation (Fig. 5b), indicating flow. Melt fragments observed by backscattered electron imaging reveal patches of varying gray value, indicative of diverse melt particle compositions (Fig. 5c).

The unit 2 breccia is supported by a groundmass that represents a mixture of microcrystalline carbonate grains and very fine-grained silicate matter (Fig. 5d). It has not been possible, even with the use of the SEM, to conclude what the nature (and origin) of this silicate material is, but it is thought that it represents, to a large degree, altered melt particles. Secondary fibrous and, as yet unidentified, minerals can be discerned at a <5 μm scale in an otherwise unresolved silicate phase. The microscopic calcite grains range in size from 10 to 40 μm. Younger, irregularly shaped carbonate veins, 0.5–2.5 mm wide, cut across the groundmass and meander around the fragments. The lithic clast content is similar to that of unit 1, comprising limestone, dolomite, shale, quartzite and quartz, granite, and schist fragments, but with significantly fewer carbonate inclusions. Rare weakly shocked feldspar fragments with kink bands and micro-shear planes have also been observed. An ~3 cm wide quartz-plagioclase-biotite-apatite-sphene schist clast occurs at a depth of 824 m. The plagioclase in this clast was melted; this melt phase is now mostly devitrified and altered.

Unit 3

Many microscopic characteristics of unit 3 are similar to those of unit 2. The most noticeable differentiating feature is the multi-colored (variegated) nature of the melt fragments in unit 3. Under plane polarized light, the dominant colors of these fragments are patchy brown and orange. Again, lath-shaped microlites are common in the melt fragments and at noticeably greater abundance than in unit 2. The melt fragments are typically sub-rounded to sub-angular and can display prominent alteration rims (Fig. 6a). The groundmass is carbonate-rich and appears similar, but slightly coarser-

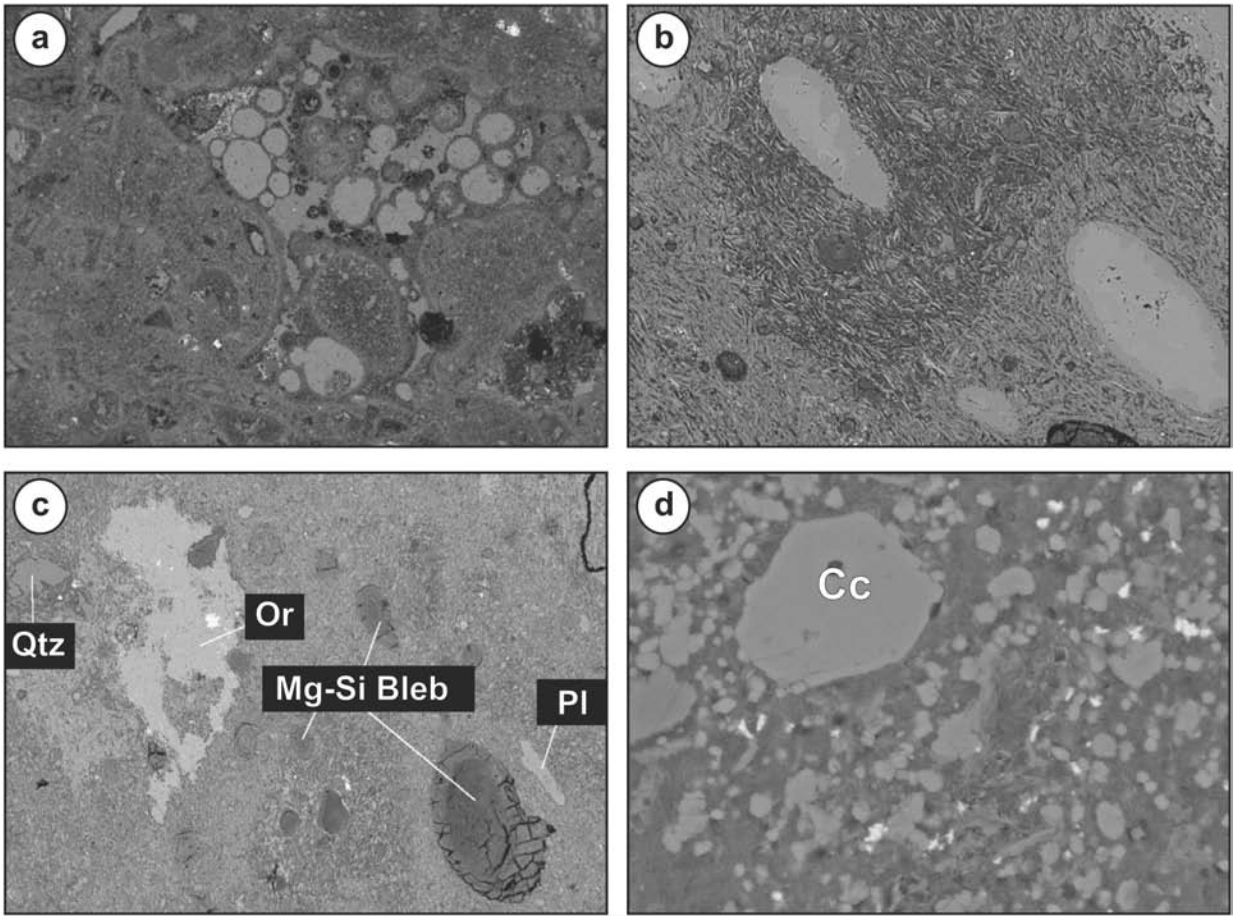

Fig. 5. Backscattered electron images (BSE) of unit 2: a) highly angular and vesiculated, melt particle-rich breccia; note that most of the vesicles in the large melt rock fragment are infilled by calcite, while remaining vesicles contain groundmass material; image width = 2.4 mm, sample depth = 835.18 m; b) primary immiscible fine-grained carbonate blebs set in a microlite-rich melt rock fragment; note the similar alignment of the blebs to the microlites; image width = 1 mm, sample depth = 844.82 m; c) microlite-bearing melt rock with magnesium-silica-rich blebs (dark ovoid), orthoclase (Or), and quartz (Qtz), as well as a partially assimilated plagioclase crystal (Pl); image width = 2 mm, sample depth = 844.82 m; d) mixed groundmass: calcite (Cc) crystals in between silicate particles; image width = 0.1 mm, sample depth = 835.14 m.

grained (0.05–0.2 mm), than that of the upper units (Fig. 6b). A similar observation—i.e., increase of matrix grain size from the uppermost unit to the second interval—was made by Claeys et al. (2003) for the impactites from the Y6 borehole. The clast population in unit 3 is the same as that described for unit 2. However, specific to unit 3, many feldspar grains have checkerboard texture (Fig. 6c). Other feldspar clasts show deformation features that are indistinguishable from those formed by conventional tectonic deformation processes, i.e., extensive fracturing that was most likely produced in a brittle deformation regime. Shock metamorphic effects in clasts are similar to those in clasts of the overlying units, but an increase in the number of sets of PDFs per quartz grain is apparent (see the section on Modal Analysis below; Table 3). Rare anhydrite blebs, interpreted here as clasts, are observed in melt fragments. They have radiating acicular growth textures (Fig. 6d), which could indicate that they are crystallized melt phases. Irregular carbonate blebs are also common in melt fragments.

Unit 4

Unit 4 has a very large (75–80 vol%) melt fragment component. These fragments usually contain abundant microlites that may be localized in specific bands. This banding is further accentuated by compositional and alteration heterogeneities (Fig. 7a; also Ames et al. 2003). In contrast to the overlying units that show a more diverse lithological variation in the clast content (see also point count analyses; Table 3), lithic and mineral clasts in unit 4 comprise primarily quartz, feldspar, and granite. Feldspar grains show signs of thermal overprint and commonly display checkerboard textures. Quartz grains have undergone

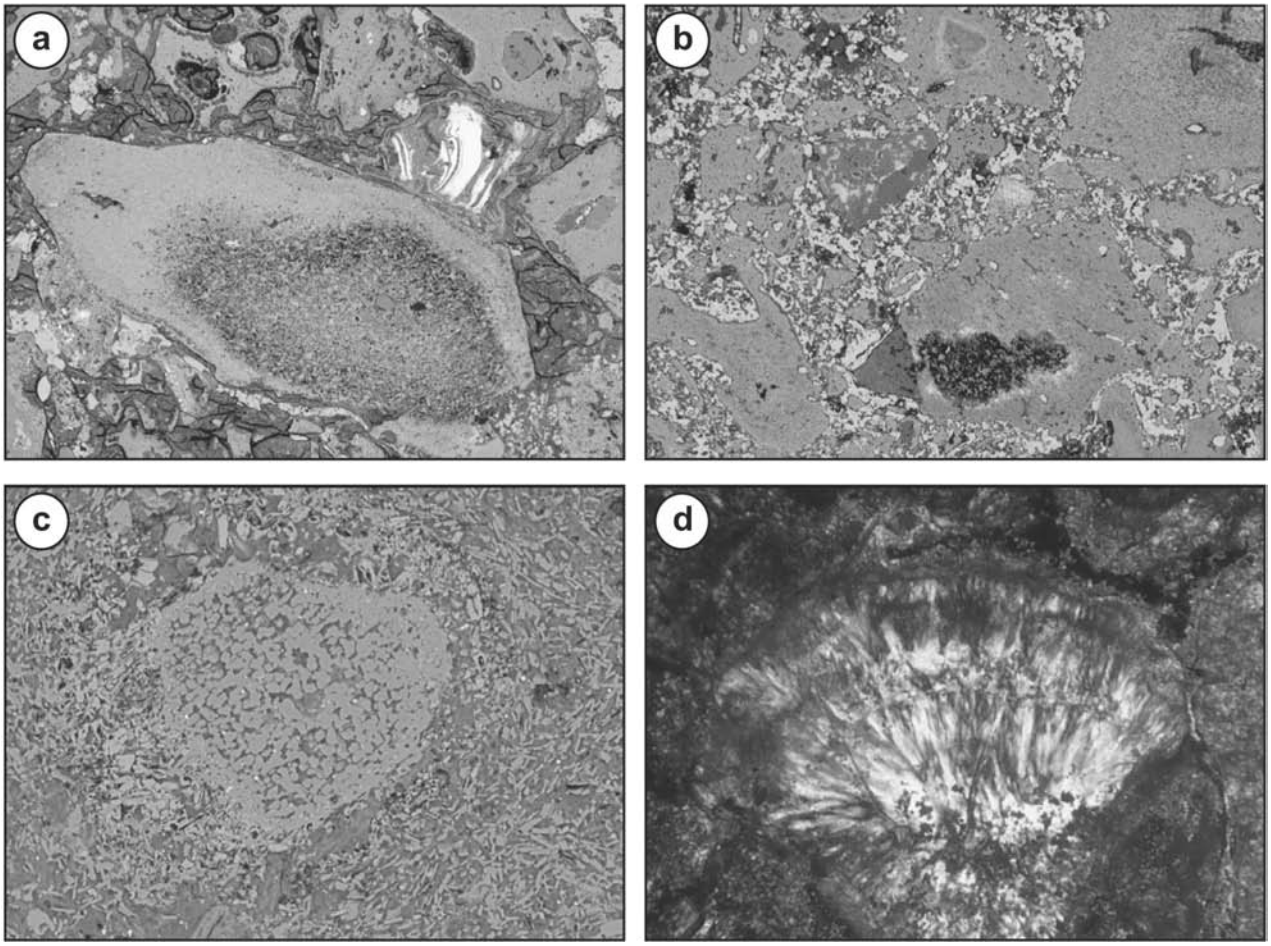

Fig. 6. Photomicrographs of unit 3: a) subrounded to subangular melt particles; notice the alteration corona surrounding the large melt particle; image width = 1 mm, sample depth = 846.80 m; b) melt particles suspended in carbonate-rich groundmass; image width = 2mm, sample depth = 851.15m; c) checkerboard plagioclase in microlite-rich melt rock; image width = 0.4 mm, BSE, sample depth = 851.15 m; d) patch of radiating crystals of anhydrite in melt rock; image width = 0.5 mm, CPL, sample depth = 846.80 m.

extensive recrystallization as observed by characteristic mosaic textures. Where recrystallization or mosaicism have not affected entire crystals, the remnants sometimes display one or two sets of PDFs. This unit is pervaded by a network of anastomosing and undulating opaque veins that are hydrocarbon-rich (Fig. 7b). Black oil was observed oozing out of some thin section cut-offs, and a distinct oily odor was detected during sample preparation. Rare green and brown blebs observed within melt fragments are thought to represent an alteration product, likely of an original mafic component. The main and most obvious alteration product of the melt particles comprises prominent, acicular crystal aggregates and veins (Fig. 7c). Zurcher et al. (2003) suggested that this phase could have been chlorite that is now altered to other phyllosilicate phase(s); our XRD study failed to detect any chlorite. Microprobe analyses and SEM observations indicate that the material in such veins comprises acicular clay minerals such as saponite. The presence of these phyllosilicate phases produces a cloudy gray overprint on many light colored melt particles. In contrast to the overlying units, veins and isolated patches of carbonate are rare to totally absent.

Unit 5

Unit 5 has the highest carbonate content of all impactite units (see Table 3). Similar to units 2 and 3, melt particles are totally suspended in a carbonate-dominated groundmass (Fig. 8a). As observed in hand samples, the melt particles are mostly subangular. The microlite content in these melt fragments is variable, ranging from abundant to totally absent (see Table 3). This is in contrast to the overlying units where microlites in melt fragments are generally of uniform abundance on a thin section scale. As in the two immediately overlying units, melt fragments contain various lithic and monomineralic inclusions, predominantly of granitoid origin, including much quartz. In the matrix, small, subrounded to

Table 3. Modal analyses of selected samples from units 1 to 5 (data in vol%).[a]

Unit		1	1	1	1	2	2	2	2	2	3	3	3
Depth (m)		803.4	805.3	810.8	821.4	825.4	827.1	835.1	840.3	843.5	846.0	846.8	851.2
Description		Sue.	Sue.	Sue.	Sue.	Sue.	Sue.	Sue.	B.M.R.	B.M.R.	Sue.	Sue.	Sue.
Melt particles, rock, and matrix	Green		1.5	9.9	1.8	1.2		0.5				0.3	
	Brown	1.9	3.7	4.0	4.7	31.4	0.4	3.3			7.4	9.2	
	Brown, microlite rich						12.0	3.3	61.5	34.8	22.2	21.4	5.4
	Yellow					0.9	12.2			3.1			1.5
	Yellow, microlite rich						8.6				2.3	0.1	0.8
	Colorless, microlite rich	0.3			1.8		11.5	17.4	19.4	20.9	17.0	16.8	34.6
	Orange/red	0.1	0.3	0.5		0.2				0.7		0.1	0.6
	Multi-colored		0.3	6.1		0.3		0.1				0.7	
	Colorless	13.7	31.4	34.3	36.0	25.2	6.5	34.0		10.2	0.1	0.8	21.6
	Perlitic fractured	39.5	18.4	18.4	5.3		1.4						
	Siliceous matrix	10.4	2.6	0.5	1.9	2.3	12.0	11.2			7.6		0.1
Carbonate	Carbonate, microcrystalline	18.7	15.7	7.7	28.4	7.0	12.0	19.8			21.3	20.0	6.6
	Carbonate crystal or patch, med.-grained	7.7	6.1	2.8	3.6	6.6	0.7	3.7	1.7	1.0		1.5	2.5
	Carbonate bleb, immiscible in glass	0.9	1.4	0.8	2.8		3.1	1.5	0.5	1.9	5.0	4.3	2.1
Carbonate/ sulfate clastic	Limestone/dolomite fragment	2.9	2.8	5.0	1.6	4.1	0.1	0.1		0.2	0.1		
	Foraminifer/shell	0.6	1.3	0.3									
	Anhydrite	0.1			0.3	0.2		0.1					0.1
	Carbonaceous siltstone		0.7	0.2		1.7		0.7				0.3	
Unshocked silicate clasts	Clinopyroxene		0.2	0.2		0.1							
	Apatite	0.1				0.1							0.1
	Opaques	0.2				2.5			0.2	0.1		0.1	
	Quartzite					0.1				6.7			0.2
	Quartz	0.3	0.5	0.2	0.6	1.2	0.7		2.3	1.5	2.9	3.6	0.6
	Feldspar	0.2				0.1				0.3			
Shocked clast content	Ballen quartz	0.4	1.3	0.1				0.3			0.3		0.4
	Quartz, 1 set of PDFs	0.2	0.2		0.1	0.1	0.5	0.1		0.6	0.1	0.2	0.7
	Quartz, 2 sets PDF of PDFs	0.1			0.1	0.1	0.6			0.2	0.2		0.3
	Quartz, 3 sets of PDFs												
	Checkerboard feldspar					0.1							
	Plagioclase with PDFs	0.7			0.3	0.1		0.4			0.2		
Secondary phases	Carbonate veining		8.6	5.6	3.1	2.6	16.0		1.4	1.8	8.9	15.0	8.2
	Opaque vein (hydrocarbon)					3.6						0.4	
	Opaque patch	1.2	3.0	3.4	7.7	4.6	1.7	3.7	12.7	12.9	3.8	3.1	1.3
	Acicular yellow crystal aggregate or bleb					8.4	0.2		0.3	2.7	0.6	2.1	12.4
Totals	Melt particles	55.4	55.6	73.2	49.6	59.1	52.6	58.6	80.9	69.7	49.0	49.5	64.5
	Microlite	0.2			0.9	0.0	16.1	10.4	40.5	27.9	20.8	19.2	20.4
	Groundmass	36.8	24.4	11.0	33.9	15.9	24.7	34.7	1.7	1.0	28.9	21.4	9.2
	Carbonate matrix	26.4	21.8	10.5	32.0	13.6	12.7	23.5	1.7	1.0	21.3	21.4	9.1
	Clastic carbonate	3.6	4.8	5.5	1.9	6.0	0.1	0.9		0.2	0.1	0.3	0.1
	Carbonate content	30.8	36.6	22.4	39.8	19.9	31.8	25.9	3.6	4.9	35.3	41.1	19.6
	Clastic silicate	2.2	2.2	0.5	1.1	4.4	1.8	0.8	2.5	9.4	3.7	3.9	2.3
	Secondary silicate & opaques	1.2	3.0	3.4	7.7	19.1	17.9	3.7	14.4	15.6	13.3	20.5	13.7
	Total	100.0	100.0	100.0	100.0	100.0	100.0	100.0	100.0	100.0	100.0	100.0	100.0

Table 3. Modal analyses of selected samples from units 1 to 5 (data in vol%).[a] *Continued*.

Unit		3	4	4 Dup.[b]	4	4	4	5	5 Dup.[b]	5	5	5	5
Depth (m)		860.4	875.8	875.8	878.1	879.0	882.5	886.8	886.8	888.1	890.5	892.6	894.1
Description		B.M.R.	G.M.R.	G.M.R.	G.M.R.	G.M.R.	G.M.R.	Sue.	Sue.	Sue.	Sue.	Sue.	Sue.
Melt particles, rock, and matrix	Green						0.1	0.3	0.9	0.8			
	Brown		0.1										
	Brown, microlite rich	9.8	0.6		0.5	11.2	2.2			0.2	6.4		
	Yellow												
	Yellow, microlite rich					0.4							
	Colorless, microlite rich	60.5	72.6	72.9	70.1	47.0	73.1	7.9	11.2	18.2	54.4	39.6	
	Orange/red												
	Multi-colored												
	Colorless	5.6	0.9	6.3	3.6	3.4	1.9	9.4	2.7			2.3	12.0
	Perlitic fractured												
	Siliceous matrix												
Carbonate	Carbonate, microcrystalline					4.0		44.2	59.3	67.5	19.7	50.0	70.2
	Carbonate crystal or patch, med.-grained	4.9				0.4	0.1	0.7	0.9	5.2	2.0	1.3	0.4
	Carbonate bleb, immiscible in glass	0.1							0.9	0.1	1.8	1.0	
Carbonate/ sulfate clastic	Limestone/dolomite fragment	0.1						18.6	15.0		1.5		10.8
	Foraminifer/shell							0.6	0.7	0.1			1.5
	Anhydrite										0.2		
	Carbonaceous siltstone												
Unshocked silicate clasts	Clinopyroxene												
	Apatite						0.1						
	Opaques		0.1				0.3	0.3					
	Quartzite												
	Quartz	2.0	0.5		1.2	2.0	0.7	4.0	1.4	0.4	1.4	0.8	
	Feldspar												
Shocked clast content	Ballen quartz	0.2	1.3	1.4	0.8	0.3					1.5		
	Quartz, 1 set of PDFs	0.6	0.5	0.6	0.2		0.5	0.3	0.3	0.2	0.1	0.1	
	Quartz, 2 sets PDF of PDFs	0.2	0.2		0.1		0.2	0.1	0.1	0.4		0.5	
	Quartz, 3 sets of PDFs	0.1	0.2			0.1		0.2	0.3	0.2		0.4	
	Checkerboard feldspar	0.2	0.4	0.8	0.6	2.4	1.4			0.1	0.2	0.1	
	Plagioclase with PDFs	0.7	0.1		0.4	2.2			0.4				
Secondary phases	Carbonate veining	2.4				0.7		6.3	0.5	0.4	4.6	0.4	0.4
	Opaque vein (hydrocarbon)	2.2	7.6	6.3	4.7	3.8	12.0	6.5	3.9	5.6	3.1	1.0	4.8
	Opaque patch	2.8	0.5	1.1	1.3	2.5	3.9		0.8	0.6	1.0	2.3	
	Acicular yellow crystal aggregate or bleb	7.6	14.7	10.6	16.5	19.7	3.5	0.6		0.2	2.3	0.1	
Totals	Melt particles	75.9	74.2	79.2	74.2	62.0	77.3	17.6	14.8	19.1	60.8	41.9	12.0
	Microlite	35.2	36.6	36.5	35.3	29.3	37.7	4.0	5.6	9.2	30.4	19.8	
	Groundmass	4.9				4.4	0.1	44.9	60.2	72.6	21.7	51.3	70.6
	Carbonate matrix	4.9				4.4	0.1	44.9	60.2	72.6	21.7	51.3	70.6
	Clastic carbonate	0.1						19.2	15.7	0.1	1.7		12.3
	Carbonate content	7.5				5.1	0.1	70.4	77.3	73.2	29.7	52.7	83.3
	Clastic silicate	4.0	3.1	2.8	3.3	7.0	3.2	4.9	2.5	1.3	3.2	1.9	
	Secondary silicate & opaques	12.6	22.7	18.0	22.5	26.6	19.4	13.5	4.7	6.8	10.9	3.4	5.2
	Total	100.0	100.0	100.0	100.0	100.0	100.0	100.0	100.0	100.0	100.0	100.0	100.0

[a]Abbreviations are: Sue. = sSuevite; B.M.R. = brown melt rock; G.M.R. = green melt rock.

[b]Note count duplication at 875.8 m and 886.8 m depths per sample.

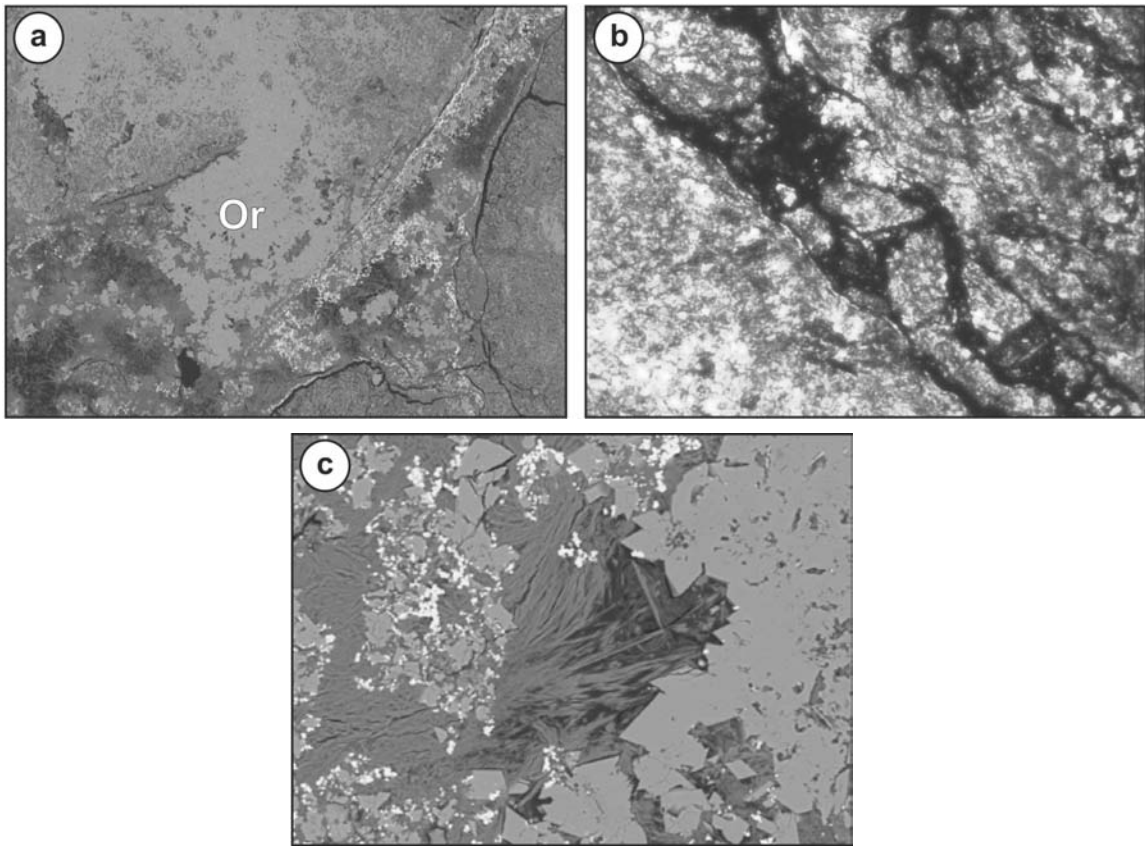

Fig. 7. Photomicrographs of unit 4: a) orthoclase (Or) secondary crystallization growth; image width = 1.5 mm, BSE, sample depth = 875.79 m; b) altered microlite-bearing melt rock with fluidal texture intertwined with dark opaque veins thought to be filled with hydrocarbons; image width = 4 mm, PPL, sample depth = 875.79 m; c) secondary acicular phyllosilicate needles (saponite) in porous vein; image width = 0.6 mm, BSE, sample depth = 875.79 m.

subangular clasts of sedimentary precursors, including dolomite, limestone, calcareous siltstone, and quartz-rich siltstone, can be discerned. The groundmass also contains granitic limestone and siltstone clasts, as well as rare limestone clasts with foraminifera microfossils. Carbonate fragments are optically almost indistinguishable from the groundmass, but they are readily discerned by cathodoluminescence (see the Cathodoluminescence section below). Backscattered electron imaging reveals that the carbonate-dominated groundmass contains numerous inclusions of quartz and barite, silicate melt particles, and euhedral dolomite crystals (Fig. 8b). The carbonate groundmass has a variable grain size, ranging from microcrystalline to fine-grained (<0.05–2 mm). It also reveals a unique texture: subangular to subrounded microcrystalline (<0.05 mm) carbonate aggregates that appear to be enclosed by larger carbonate crystals, similar to a poikilitic texture in igneous rocks. The apparent host crystals can be in optical continuity for up to 2 mm and display interlocking grain boundaries (Fig. 8c). This texture could, of course, represent a sedimentary feature of target carbonates resulting from dissolution and recementation. Vesicles in melt clasts contain euhedral barite growths, and occasionally, vugs are observed that are rimmed by iron oxides.

Brown Melt Fragments

Brown melt fragments (up to >10 cm in size) occur throughout the breccia package but are most abundant at the base of unit 3. They are found sporadically, though in increasing numbers with depth, throughout unit 2 but only occur as small and rare fragments in unit 1. As with other melt fragments found in units 2 to 4, the brown melt fragments are also fluidal-textured and have angular morphologies and commonly contain abundant microlites that are typically flow-aligned. Schlieren occur commonly as brown patches that may appear totally opaque and that enclose small tabular microlites of pyroxene and feldspar. Rounded and ovoid carbonate blebs, 0.5 to 3 mm in size, and small monomineralic inclusions (mostly quartz and plagioclase) are also found within this melt. The brown melt particles at the base of unit 3 texturally resemble the green monomict melt breccia of unit 4. Melt fragments locally fit together in a jigsaw puzzle-like arrangement.

Shock Metamorphism

Numerous clasts in the impactites of the Yax-1 borehole display shock metamorphic features. Quartz grains with planar deformation features (PDFs) are ubiquitous. They are

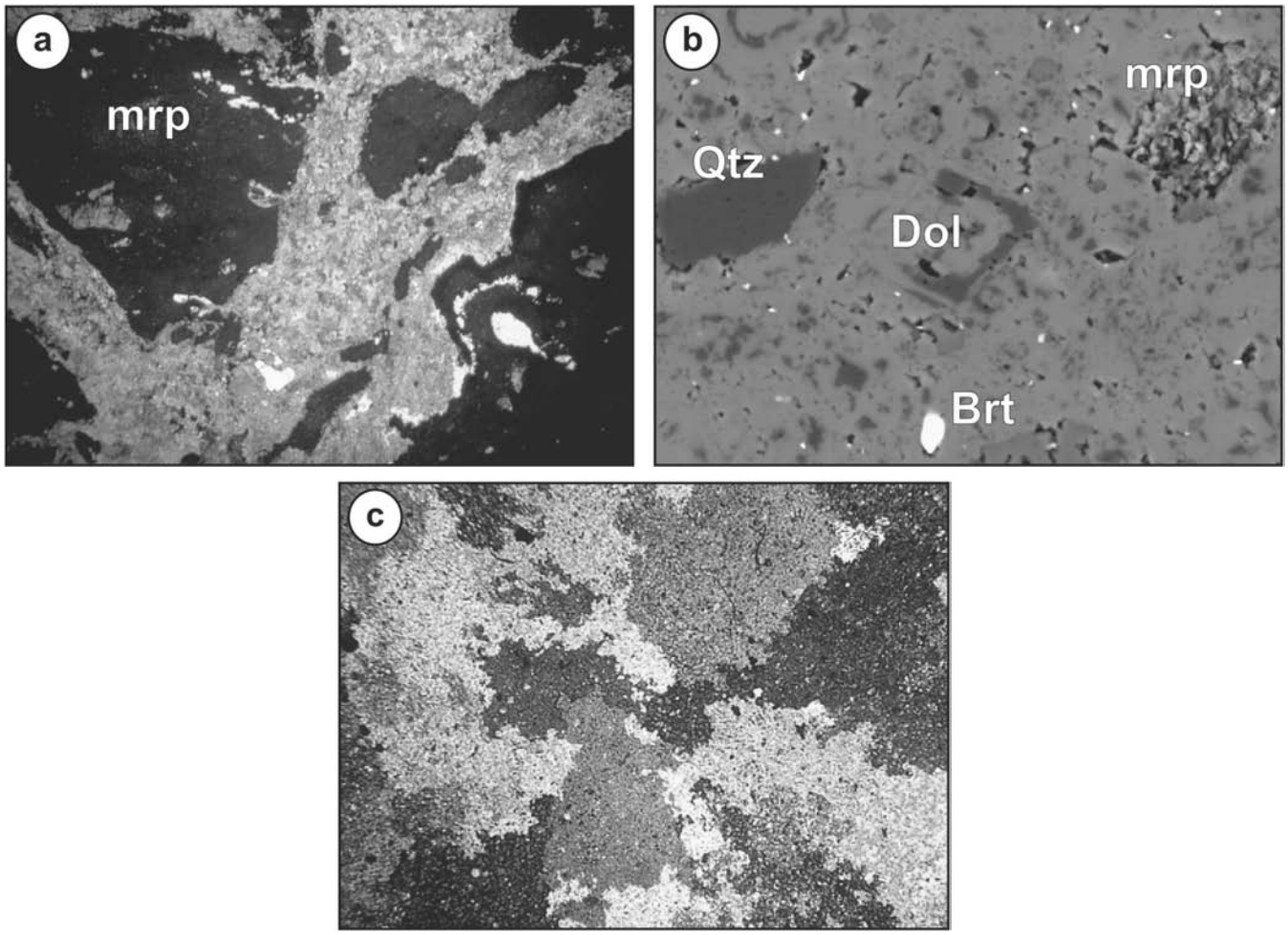

Fig. 8. Photomicrographs of unit 5: a) semi-isotropic melt rock particles (mrp) set in microcrystalline carbonate groundmass; image width = 5 mm, CPL, sample depth = 892.55 m; b) carbonate groundmass showing numerous microscopic inclusions of melt rock particles (mrp), quartz (Qtz), and barite (Brt), with a euhedral dolomite (Dol) crystal; image width = 0.19 mm, BSE, sample depth = 892.55 m; c) carbonate groundmass with interlocking, internally fine-grained calcite patches, scale = 1 mm, CPL, sample depth = 886.79 m.

generally found as small grains, 1–5 mm in size, and typically have 1 to 3 sets of PDFs (Fig. 9a) that are indicative of shock pressures of 15 to ~30 GPa (e.g., Stöffler 1974; Langenhorst and Deutsch 1994; Huffman and Reimold 1996). Point count analyses indicate that the proportion of quartz grains with multiple sets of PDFs appears to increase with depth in the impactite interval (Table 3). Ballenquartz (Fig. 9b) forms <1.5 vol% in samples from all units. If ballenquartz is the result of recrystallization of diaplectic glass, it indicates a minimum shock pressure of about 30 GPa (Bischoff and Stöffler 1984). Unit 4, however, appears to contain more ballenquartz and checkerboard-textured feldspar particles than the other units (cf., Table 3). Checkerboard-textured particles reveal remnants of both plagioclase and alkali feldspar precursors. Bischoff and Stöffler (1984) suggested that the checkerboard texture reflects preferential melting along important crystallographic orientations in feldspars and was indicative of shock pressures in excess of 35 GPa.

A large granitic clast was observed within unit 5 at a depth of 889.59 m. All plagioclase and feldspar minerals show partial isotropization, occasional PDFs, and undulating contacts indicative of melting. Quartz minerals are rare but can reveal two to three sets of PDFs and extensive mosaicism (recrystallization). Amphibole crystals have also been observed and reveal shattered and highly fractured morphologies. Apatite crystals have been observed under cathodoluminescence and appear unshocked.

The most striking characteristic of the Yax-1 impactites is the high proportion of melt fragments. A few fragments still preserve evidence of the crystalline precursor material, as seen in relict polysynthetic plagioclase twins in small parts of such clasts. As discussed below (see Electron Microprobe Analysis section), both individual mineral and mineral combination compositions are represented in this melt component. Thus, this component represents the entire shock pressure range between mineral melting (from ~35–40 GPa shock pressure) and bulk rock melting (from ~50 GPa) (Bischoff and Stöffler 1984).

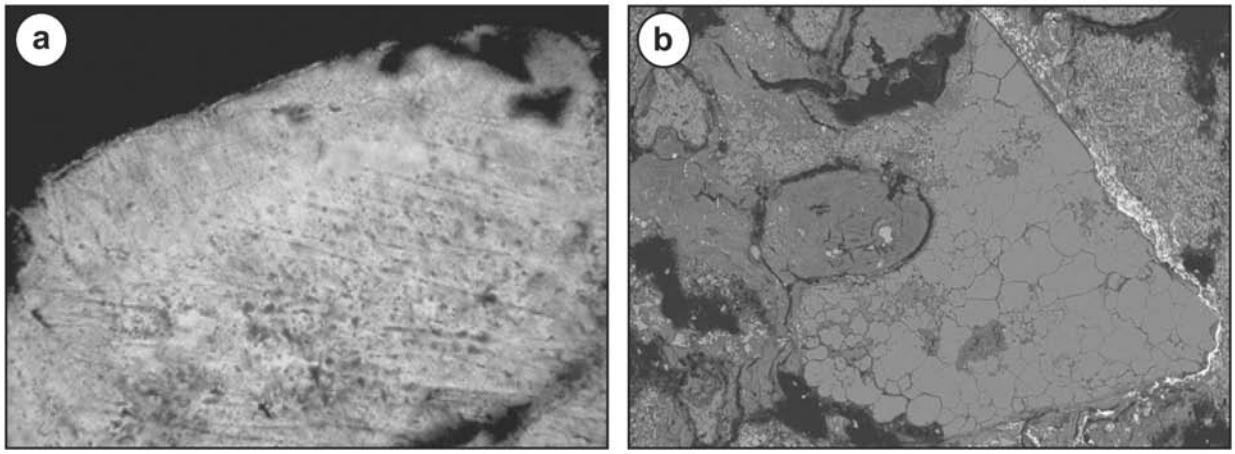

Fig. 9. Shock metamorphic features: a) shocked quartz grain with 2 sets of PDFs; image width = 0.45 mm, CPL, sample depth = 892.55 m; b) ballenquartz in microlite-bearing melt rock fragment; note narrow (bright) iron-oxide rim around the grain and the phyllosilicate-rich vesicle infill to the center-left of the image; image width = 1.15 mm, BSE, sample depth = 878.09 m.

Modal Analyses

The results of modal analysis by point counting of selected thin sections from each unit of the impactite sequence are presented in Table 3. The major components identified are melt particles, various lithic and mineral clast types, and secondary phases. Among the clastic component, carbonate, silicate, and shocked silicate inclusions have been distinguished. From Table 3, it is obvious that the various samples of a specific unit have highly variable modes. This is obviously related to the small sample sizes that are clearly not representative of these varied lithologies.

Various types and proportions of melt particles are found throughout the impactites. Altered green melt, predominantly with intense perlitic fracturing, is the important type in unit 1. Orange/red and uniformly devitrified melt particles are restricted to units 1 to 3. Microlite-bearing melt particles are dominant in units 2 to 5. An increase in the proportion of brown melt particles in the suevite samples occurs with depth, but they are totally absent in unit 5. Large microlite-bearing brown melt particles occur at depths of 840.3 m and 843.5 m in unit 2 and at a depth of 860.4 m in unit 3. Unit 4 has the highest abundance of microlite-bearing melt.

Several trends are observed with respect to the clast content. Lithic carbonate inclusions are found predominantly within unit 1 (1.9 to 5.5 vol%), in one sample in the upper segment of unit 2 (depth of 825.4 m, 6 vol%), and in unit 5 (0.1 to 19 vol%). Foraminifera are only found in these samples. Anhydrite fragments are rare and are restricted to units 1 and 2. Siliceous clasts (shocked and unshocked) occur throughout the impactites; unit 4 samples have characteristic checkerboard feldspar.

Carbonate veins and blebs in melt fragments (the blebs possibly representing vesicle infilling) occur in all units besides unit 4. The brown and green melt-rich samples in units 3 and 4 reveal extensive alteration in the form of veins and patches filled by fine-grained acicular crystals. Dark, opaque patches were found throughout the impactite sequence and may represent hydrocarbon-bearing material with oxide alteration products.

Various totals are tabulated at the bottom of Table 3. The total melt particle value represents the sum of melt fragment abundances. The microlite total is determined on the assumption that their mean abundance equals half that of the microlite-bearing melt rock particles (cf., Fig. 5c). While the microlite values presented in Table 3 only constitute estimates, their relative variation from unit to unit appears meaningful. For the carbonate matrix total, the proportions of the fine- and medium-grained carbonate groundmass were added. The clastic carbonate value is a straightforward addition of all the clastic carbonate components. The total carbonate content is the sum of the matrix, clastic, and secondary carbonate components, and the clastic silicate total is the sum of all monomineralic and lithic silicate components. It is important to note that the tabulated results measured from thin sections 840.3, 843.5, and 860.4 m actually represent large particles of brown melt and are, therefore, not representative of the unit that they have been grouped with.

Overall trends can be inferred from the tabulated totals. The total melt particle content from units 1 to 3 is highly variable, ranging from 49 to 73 vol%. The massive brown melt particles and the unit 4 samples gave the highest melt contents, ranging from 70 to 81 vol%, with one highly altered sample containing 62 vol%. In contrast, unit 5 has the most variable melt particle content with values ranging from 12 to 61 vol%. Groundmass proportions in the suevites are also highly variable. Units 1 to 3 have a groundmass content ranging from 11 to 37 vol%. The unit 4 and brown melt particle samples contain minor proportions of groundmass due to their massive nature, ranging from 0 to 5 vol%. The groundmass proportions of units 1 to 3 and 5 correlate

negatively with the melt content, ranging from 22 to 73 vol%. Because of the multi-component nature of the groundmass in units 1 to 3 (Fig. 5e and 5f), the calcite grain, siliceous matrix, and lithic mineral fragment constituents have been tabulated according to the corresponding major components. The total carbonate content fluctuates between 4 and 41 vol% in unit 1, is almost completely absent in unit 4, and varies strongly in unit 5 between 30 and 83 vol%. In unit 5, most of the carbonate is found in the groundmass. The total clastic silicate and secondary silicate contents are generally high throughout the impactites. It is important to note that these modal proportions, especially with regards to the carbonate content, provide not only a basis for discussion of mixing of different melt and target rock components but also for the discussion of geochemical trends (e.g., Tuchscherer et al. 2004).

Electron Microprobe Analysis of Melt Phases

Electron microprobe analyses were performed on a large number of melt fragments in 10 samples from units 2 to 5. The samples analyzed are from depths of 827.13 m (2 sections), 835.18 m, 844.82 m, 846.01 m, 860.40 m (2 sections), 878.09 m, 890.52 m, and 892.55 m. As shown in Fig. 10 and Tables 4 and 5, the analyses cover a wide range of compositions. Because altered melt particles should have high volatile contents, only the results with weight percent totals close to 100 wt% are considered to represent reasonably unaltered material. Alkali element- and silica-rich melt particles have varied concentrations of SiO_2 (54–67 wt%), TiO_2 (0–2.8 wt%), Al_2O_3 (17–27 wt%), FeO_{tot} (0–3.55 wt%), MgO (0–2.35 wt%), CaO (0–10 wt%), Na_2O (0–11 wt%), and K_2O (0–16 wt%) (only those results that yielded total weight percent values between 97 and 103 wt%). Small amounts of iron and magnesium are present in many of the alkali element-silica-rich melts. Mafic melt particles generally have a high volatile content and, thus, low analytical totals. The electron microprobe analyses indicate that these particles also commonly have high proportions of alkali elements—up to 5 wt% Na_2O and CaO and up to 10 wt% K_2O, despite high FeO_{tot} (i.e., Fe as FeO) and MgO contents.

Selected major oxides were converted into molecular proportions and plotted on a modified four-component ACF-A'FK diagram (after Eskola 1939; Fig. 10). Modifications to the methodology of Eskola (1939) were required because the total iron content is plotted in the F apex instead of only the ferrous iron (Fe^{2+}) content. Phosphorus was not analyzed, and thus, the C apex does not incorporate this component. The apices are defined as follows: A and A' = Al_2O3 – (Na_2O + K_2O), C = CaO, F = FeO_{tot} + MgO + MnO, K = K_2O. Although the diagram was originally intended for metamorphic rocks, it can serve to compare the melt fragment compositions with those of possible precursor minerals.

The already mentioned strong variability of compositions is obvious in Fig. 10. Most analyses fall into two broad trends, namely, mafic and alkaline. Note the heterogeneous composition of the melt particles. Heterogeneity (mixing) in the ACF diagram is observed primarily between the A and F apex. In the A'FK diagram, alkali-rich melt particles plot throughout the ternary diagram. Mafic melt particles cluster toward the F apex in both diagrams of Fig. 10a. Alkali element-rich melt particles, on the ACF diagram, also fall onto a strong trend that produces a constant ratio of molecular calcium oxide toward the A and F apices, clustering between 40 and 50 mol%. In the A'FK diagram, alkali element-rich melts scatter throughout the ternary diagram but plot notably away from the F apex, where a distinct grouping of mafic compositions is located. As the diagram does not account for silica, the analyses do not represent any quartz-derived melt or melt compositions with significant silica admixture. It is, however, important to note that, to date, no silica-rich melt that could be derived from a predominantly quartz precursor or that incorporated a significant quartz component has been analyzed (the highest SiO_2 contents measured are on the order of 60–63 wt%).

The distribution of the melt analyses, against the rock types known to have been sampled in the clast contents of impactites, i.e., carbonates, granitoids, and amphibolites (Kettrup et al. 2003), as well as some sedimentary and metamorphic rocks such as siltstones and schists (this study), indicates that the precursor minerals included primarily feldspars, amphibole (a likely Ca contributor), biotite, muscovite, and, presumably, quartz. Our petrographic analysis did reveal the presence of traces of clinopyroxene in the clast content but at minute proportions. The compositional boundary observed above 50 mol% C, in the ACF diagram, suggests that no mixing occurred between alkali element-rich melt and extensive amounts of calcium carbonate or sulfate (in agreement with the petrographic observation of possible exsolution of carbonate melt blebs from silicate dominated melt).

Considering the petrographic finding that melts generally are strongly altered and/or devitrified and as many totals of the EMP analyses fall far short of 100 wt%, it must be established whether the trends identified in Fig. 10a are significant or are the result of secondary overprint. As two data sets were collected, with electron beam widths of 10 and 3 μm, respectively, we had to investigate whether or not beam size effects play a role. It became obvious, however, that this is not the case. The two different data suites display similar trends. When plotting only the analyses that have totals between 97 and 103 wt%, it can be shown that all mafic melts are eliminated from the ACF and A'FK diagrams (Fig. 10b). Obviously, all mafic melts are highly altered (see also Table 4). This is expected, as mafic minerals (biotite, amphibole, pyroxene) or, as in this case, melts are the first to undergo alteration and weathering when exposed to extensive hydrothermal activity (e.g., Freyssinet 2000). Mafic minerals are also the first to react with meteoric waters. However,

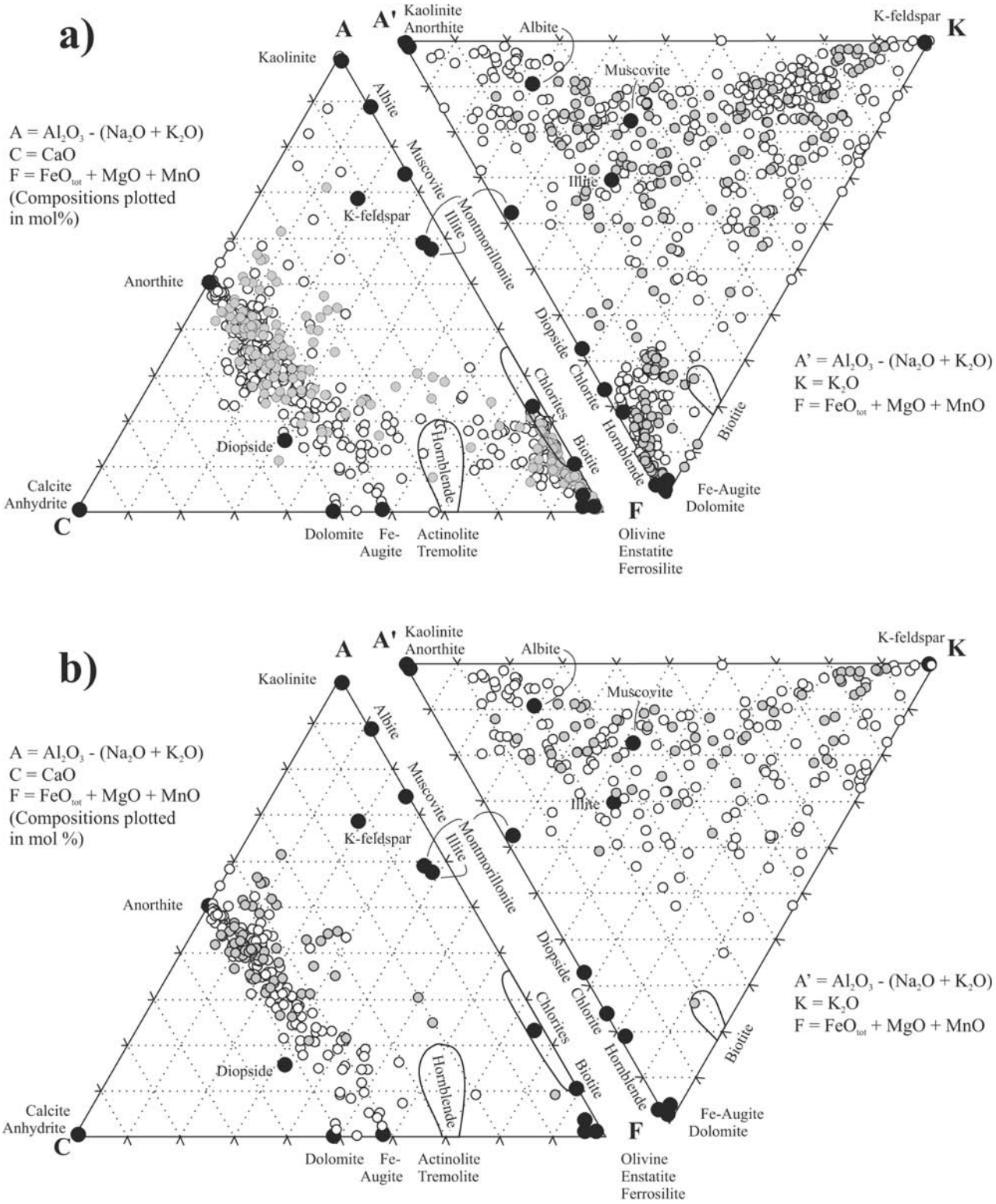

Fig. 10. ACF and A'FK diagrams (after Eskola 1939) with Yax-1 melt particle compositions (electron microprobe analyses); the plots are based on molecular proportions: a) plot showing all melt particle analyses (n = 555): gray circles represent focused beam analyses with 3 μm beam diameter, white circles represent defocussed beam analyses at 10 μm beam diameter; b) plot showing only melt particle analyses with weight percent totals between 103 and 97 wt% (n = 202). Note that none of the mafic analyses illustrated in (a) is retained, as all of these have totals <97 wt%—indicative of extensive secondary alteration.

Table 4. Averaged electron microprobe analyses of various melt particle types (data in wt%).[a]

	1. Green melt particle		2. Green melt particle		3. Green melt particle		4. Brown melt particle		5. Green melt particle		6. Beige melt particle	
Depth (m)	827.13		827.13		827.13		860.4		878.09		892.55	
Beam width	10 µm		10 µm		10 µm		10 µm		10 µm		3 µm	
	Avg. (n = 20)	2σ	Avg. (n = 14)	2σ	Avg. (n = 33)	2σ	Avg. (n = 25)	2σ	Avg. (n = 16)	2σ	Avg. (n = 20)	2σ
SiO_2	60.51	0.82	56.97	3.55	50.09	0.66	58.43	0.57	51.78	4.50	59.35	5.47
TiO_2	0.73	0.26	0.77	0.54	0.48	0.06	0.28	0.17	0.71	0.87	0.52	0.66
Al_2O_3	18.70	0.76	20.10	0.69	15.24	0.38	21.23	0.57	15.85	2.73	18.00	1.29
Cr_2O_3	n.d.	n.d	n.d.	n.d	0.01	0.01	0.01	0.01	n.d.	n.d	0.08	0.26
FeO_{tot}	1.05	0.22	4.23	2.43	5.19	0.32	1.67	0.19	2.43	0.78	5.05	6.68
MnO	n.d.	n.d	0.03	0.03	0.01	0.01	n.d.	n.d	n.d.	n.d	0.03	0.05
MgO	1.23	0.43	0.33	0.11	6.52	0.40	0.57	0.24	3.76	2.02	0.19	0.22
CaO	4.36	0.82	4.32	1.28	0.75	0.27	5.43	0.61	4.39	1.58	0.88	0.13
Na_2O	1.31	0.33	2.34	1.22	0.47	0.14	3.87	0.74	1.47	0.55	1.18	0.17
K_2O	11.17	1.01	1.76	0.92	3.83	0.23	7.10	0.76	7.05	2.08	12.66	1.26
Total	99.06		95.76		82.58		98.58		87.45		97.95	

[a]n.d. = not detected.

Table 5. Averaged electron microprobe analyses of microlite, host altered melt, and checkerboard plagioclase (data in wt%).[a]

	1. Plagioclase microlites		2. Host melt		3. Checkerboard plagioclase	
Depth (m)	890.52		890.52		878.09	
Beam width	3 µm		3 µm		10 µm	
	Avg. (n = 38)	2σ	Avg. (n = 20)	2σ	Avg. (n = 26)	2σ
SiO_2	54.43	0.26	43.31	0.50	57.39	1.42
TiO_2	0.10	0.07	0.19	0.08	0.27	0.24
Al_2O_3	25.88	0.35	8.23	0.83	24.09	1.18
Cr_2O_3	n.d.	n.d.	0.01	0.01	n.d.	n.d.
FeO_{tot}	1.72	0.10	5.58	0.77	1.28	0.29
MnO	n.d.	n.d.	n.d.	n.d.	n.d.	n.d.
MgO	0.51	0.13	17.88	2.00	0.26	0.33
CaO	10.02	0.32	1.03	0.17	6.79	0.88
Na_2O	5.07	0.13	0.42	0.28	3.79	0.45
K_2O	0.57	0.09	1.12	0.38	5.15	1.13
Total	98.32		77.77		99.03	

[a]n.d. = not detected.

element mobility during weathering favors the removal of alkali elements, silica, and Mg^{2+} ions, while Al and Fe^{3+} typically remain behind as relatively inert cations (e.g., Righi and Meunier 1995).

When all melt compositions (in wt%) are plotted onto an AFM diagram (Fig. 11a), these data also reveal the characteristic divide between mafic and alkali-rich compositions. Two distinct trends are observed that suggest A plus F + M mixing and M plus A + F mixing (i.e., A = Na_2O + K_2O, F = FeO_{tot}, M = MgO). When the mafic melt compositions are plotted on a (Na + Ca)-Fe-Mg ternary diagram (Fig. 11b; see also Table 4), no extensive mixing between the alkaline and the mafic components is obvious. When the mafic melt compositions are plotted on a K-Fe-Mg ternary (Fig. 11c), a distinct linear compositional trend is observed that corresponds to K-metasomatism, with K substituting for a constant proportion of Fe^{2+}.

The composition (in mol%) of feldspathic melts is presented on an An-Ab-Or plot (Fig. 12a). Several feldspar microlites (Fig. 12b, in a sample at 890.52 m) were analyzed in relatively less-altered melt fragments. In addition, two checkerboard plagioclase crystals (Fig. 12c) were analyzed in a sample from a depth of 878.09 m. The averaged microlite and checkerboard compositions are given in Table 5 (analyses 1 and 3, respectively). A hydrated mafic melt (analysis 2 of Table 5) hosts the analyzed microlites. The feldspathic melts have compositions of $An_{<50}$ (Fig. 12a) but exhibit a rough trend toward the Or apex. This could be indicative of either the strong K-metasomatism, also shown by the mafic melts (Fig. 11c), or variable K-feldspar and plagioclase mineral melt mixing. A few analyses plot at ~An_{20}; they were obtained along a traverse of 10 melt analyses in a sample from a depth of 827 m. The albitic compositions indicate the composition of the pre-cursor plagioclase mineral.

Conversely, it can be deduced that mineral melt mixing was not pervasive.

Individual microlite analyses from the sample from a depth of 890 m (unit 5) are shown in the ternary feldspar diagram of Fig. 12b. All results fall into a tight group around An_{55}. The average composition of microlites analyzed in this study is $An_{51}Ab_{46}Or_3$ and falls within the range of feldspar microlite compositions for unit 5 samples reported by Kring et al. (2003a, b). The microlites analyzed do not appear to be extensively altered, as indicated by the good totals and the rather low mol% Or content (low K content, precluding extensive K-metasomatism).

Electron microprobe analyses of two checkerboard plagioclase crystals yielded unusual "feldspar" compositions. When the data are plotted on an An-Ab-Or diagram, it is observed that the tiny melt pockets produced from a primary plagioclase crystal of $An_{52}Ab_{48}$ composition are characterized by a significant potassium content (Fig. 12c) but with the original An:Ab ratio preserved. The diameter of the electron beam used for these analyses was about 10 μm, and, thus, it is not impossible that some of these results represent mixtures of the remnant crystalline material plus interstitial melt (compare Fig. 6c). But, this does not affect the interpretation of these data. These results are in agreement with observations on checkerboard plagioclase grains from the Lappajärvi impact crater, where an increase in K_2O and SiO_2 and a decrease in Na_2O were discerned (Bischoff and Stöffler 1984). These authors determined—based on theoretical, compositional, and textural observations—that checkerboard plagioclase grains formed above the solidus temperature of the impact melt and could reach thermal equilibrium in the span of one to two hours.

It is interesting to note that probe analyses on shocked feldspar clasts from the Y6, Y2, and Y5A drill cores, as well as feldspar grains from the Raton basin of New Mexico, do not show anorthite contents exceeding An_{58} (Izett 1990; Sharpton et al. 1996). The An concentrations reported here also fall into this plagioclase compositional range.

Electron Microprobe Traverses Across Melt Fragments

A dozen melt particles were analyzed by EMPA along traverses across entire particles, in samples at various depths (805.34, 810.84, 827.13, 835.18, 843.46, 844.82, 846.01, 846.08 851.15, 860.04, 860.40, 886.79, 878.09, 890.52, 892.55). The selected melt fragments are all characterized by differently colored schlieren. All traverses show that these fragments have highly heterogeneous compositions, with quite variable totals (65 to 103 wt%) measured from schlieren to schlieren. In general, low totals correspond to high iron and magnesium contents, which, in turn, are generally—but not always—correlated. Several fragments yielded good totals throughout; they had variable alkali element and calcium contents. Other fragments revealed that a substantial amount of iron and magnesium was mixed with the feldspathic component. Several mafic melt fragments were observed to contain unusual K abundances (3 to 5 wt%).

It was determined that the distinctive zonation in the melt particle shown in Fig. 6a is characterized by variable alkali element and CaO concentrations; both zones yielded good wt% totals (~98 wt%). The results for this grain suggest remobilization of alkali elements and Ca toward the periphery of the particle. On one occasion, a uniform and clearly pristine composition was observed for a particle that appears to have a characteristic orthoclase composition (K_2O = 14 wt%) with low Na_2O (~1 wt%) and CaO (~0.8 wt%) contents.

Overall, these traverse data emphasize that alteration—especially of mafic schlieren—has had a major effect on the melt fragments in these impact breccias. K-metasomatism is variable but widespread. The melts analyzed have highly variable compositions with melt formation from individual minerals (K-feldspar, biotite) or mineral combinations (e.g., feldspar plus a mafic mineral). The particles analyzed do not represent homogenized melt but have different compositions from spot to spot or schlieren to schlieren on a ~0.01 mm scale.

Electron Microprobe Traverses Across Carbonate Groundmass

Two traverses were analyzed across carbonate groundmass in unit 2 and 5 samples. The unit 2 groundmass represents a mixed carbonate/silicate groundmass as shown in Fig. 5e. The SiO_2 and CaO contents are highly variable and are negatively correlated (i.e., the higher the silica, the lower the calcium oxide, and vice-versa). Regions of high CaO produce the lowest oxide totals, as expected for carbonate analyses. Relatively high concentrations of Na_2O and K_2O are observed in high-SiO_2 areas, indicating a feldspathic component. Ca and Mg typically are not correlated, as one would expect if a dolomite component were present. The unit 5 groundmass reveals a generally higher CaO content than that in unit 2 groundmass. Discrete SiO_2 peaks, correlated with Al_2O_3, Na_2O, K_2O, and relatively high oxide totals, are observed locally and represent small melt fragments or lithic clasts (as imaged in Fig. 8d). Some of the magnesium peaks that do not correlate with SiO_2 or Al_2O_3 could represent isolated dolomite crystals (compare Fig. 8d).

X-Ray Diffraction Data

Bulk powders of 22 impactite samples were subjected to X-ray diffractometry. These samples included one from the upper reworked limestone interval (791.71 m), nine samples from unit 1 (800.35 m, 805.34 m, 809.00 m, 809.70 m, 811.55 m, 815.80 m, 816.62 m, 821.39 m), four from unit 2 (825.43 m, 835.14 m, 835.18 m, 840.30 m, 843.46 m), two from unit 3 (851.15 m, 860.40 m), two from unit 4 (875.79 m, 882.45 m), and four from unit 5 (886.79 m, 888.92 m—two subsamples, 890.52 m). In general, highly variable proportions of calcite and dolomite are indicated, with calcite

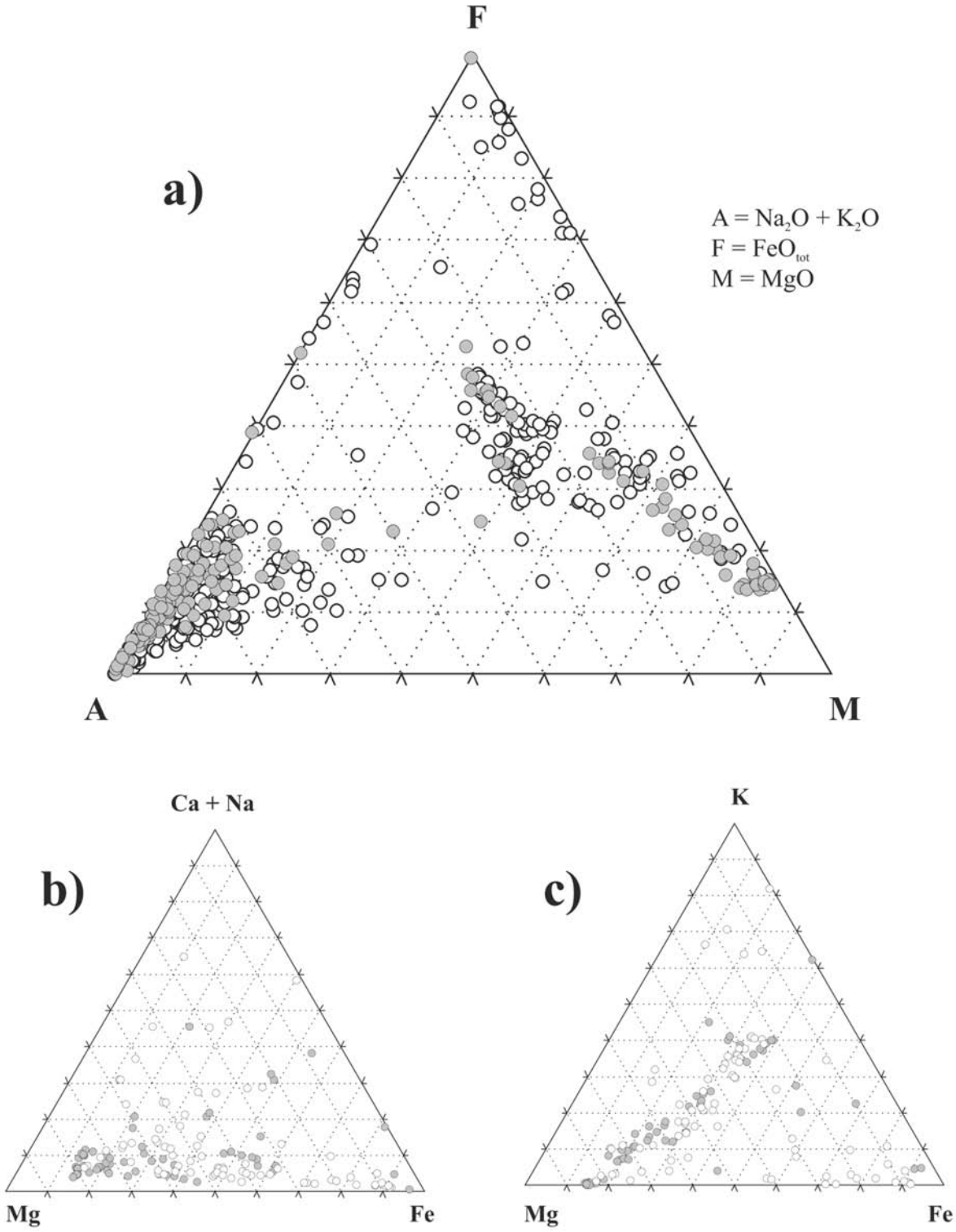

Fig. 11. a) AFM diagram of all the Yax-1 melt particle analyses (n = 555): Gray circles represent focused beam analyses with 3 μm beam diameter, white circles represent defocussed beam analyses with 10 μm beam diameter. The plot is based on weight percent results. See text for discussion; b) ternary diagram showing the mafic melt particle analyses (n = 139) according to their Fe-Mg-Ca + Na contents. Notice the lack of a strong Ca + Na overprint; c) ternary diagram showing the mafic melt particle analyses (n = 139) according to their Fe-Mg-K contents. Note the distinct trend toward elevated K contents.

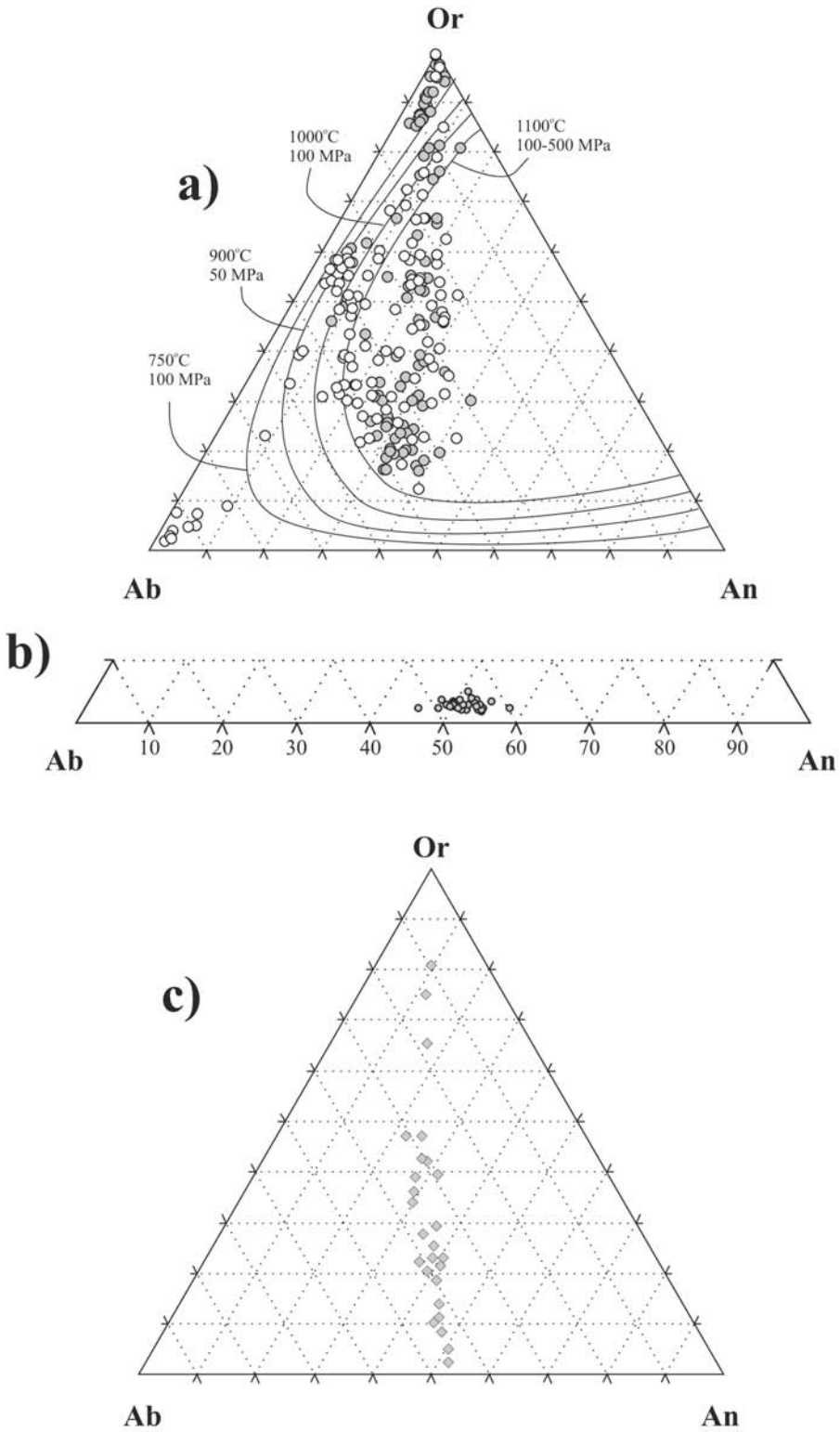

Fig. 12. An-Ab-Or diagram illustrating the composition of various feldspathic melt particles, microlites, and a checkerboard feldspar grain: a) An-Ab-Or diagram of all alkali-rich melt particles with good totals between 103 and 97 wt% (n = 202). Note that the analyses all plot on the left of the ternary with compositions restricted to $An_{<50}Ab_{0–100}Or_{0–100}$; contours after Fuhrman and Lindsley (1988); b) portion of the An-Ab-Or diagram with plagioclase microlite compositions that cluster between An_{50} and An_{56} (labradorite); c) An-Ab-Or diagram with checkerboard plagioclase compositions. Note the strong trend toward the Or corner, with a constant An/Ab ratio that would correpsond to a primary plagioclase composition of ~An_{52}.

usually dominant. An additional minor carbonate phase identified in the upper reworked limestone is ankerite. Besides calcite and dolomite, unit 1 samples reveal the presence of a phyllosilicate phase, likely an illite/montmorillonite/sepiolite at 7.07° 2θ, obviously representing the product of alkali and mafic melt alteration. Other minor phases identified are quartz, plagioclase, orthoclase, mica group minerals (biotite and muscovite), and traces of ilmenite. Unit 2 contains the same minerals but also minor pyrite. Samples from unit 3 contain the same minerals as the overlying units; however, relatively more plagioclase feldspar is present than in units 1 and 2. Unit 4 samples displayed distinct spectra with the main quartz and feldspar peaks having very similar intensities and being dominant over those for calcite and dolomite. This is in agreement with the modal analyses of unit 4 samples that indicate relatively small (<5.1 vol%) carbonate contents (compare Table 3). The phyllosilicate peaks (illite/smectite and sepiolite) are also very strong for these samples, consistent with the generally strong devitrification or alteration of melt particles. Unit 5 samples yielded variable XRD spectra, as the melt and carbonate contents are clearly variable (see Table 3). However, the calcite peak intensity always dominates over the intensities of main peaks for all other phases. Dolomite and feldspar peaks are also quite strong, while the phyllosilicate peaks are subdued.

Chlorite peaks were not detected by our XRD analysis, in keeping with our petrographic observations, as well as in agreement with Zurcher et al. (2003), who suggested that all chlorite possibly formed during alteration of melt was transformed to other phyllosilicate phases (e.g., saponite).

Cathodoluminescence Observations

Several samples were studied with cathodoluminescence (CL) microscopy. This included one sample from the sedimentary rocks above the impactites (from a depth of 791.71 m), three from unit 1 (809.7 m, 818.33 m, 821.39 m), three from unit 2 (824.03 m, 840.30 m, 843.46 m), one from unit 3 (851.15 m), three from unit 4 (875.79 m, 879.03 m, 882.45 m), and two from unit 5 (886.79 m, 888.09 m).

The upper limestone sample revealed typical orange luminescence, a characteristic of calcite (e.g., Marshall 1988). The calcite crystals contain disseminated, small (~0.1 mm), euhedral, non-luminescent rhombohedra zones (Fig. 13a). The calcite rims reveal variable intensities of orange luminescence, suggesting episodic overgrowths. Foraminifera fossils typically <0.2 mm in diameter are present locally (Fig. 13a).

Several distinctive features were observed in the unit 1 samples. As in the upper sedimentary rock, foraminifera fossils are present but are much more scarce (Fig. 4d). They have rather variable sizes, ranging from 1 to 0.1 mm. Cathodoluminescence was useful for identification of the foraminifera, as a strong alteration overprint made them almost invisible in optical microscopy. Secondary calcite veins are also more visible by this method, as they are characterized by a stronger orange luminosity with respect to the host material. This higher luminescence intensity is attributed to the paucity of "quenching" cations, such as iron, that typically subdues the luminescence of calcite (Meldin 1963). Melt particles are typically non-luminescent, however, rare green and faint blue luminescent flow textures and minerals are sometimes observed (Fig. 13b). As observed in optical microscopy, cathodoluminescence also shows that some melt particles contain carbonate blebs that may be preferentially aligned, indicative of flow.

Units 2 and 3 reveal similar cathodoluminescence features. Bright orange luminescent secondary calcite veins are observed cutting through a heterogeneous groundmass that comprises a mixture of carbonate, siliceous material, and silicate clasts (Fig. 13c). The clasts do not show luminescence, while the carbonate in the groundmass commonly shows light orange luminescence. As in unit 1, secondary veins are of stronger orange luminosity. Melt fragments in these units contain well-preserved green luminescent crystals (Fig. 13c). This CL color is characteristic of apatite, with Mn^{2+} as the principle activator that produces a broad emission band between 562 nm and 580 nm. This has been shown to be diagnostic of apatite crystals of various igneous, hydrothermal, and metamorphic origins, as well as synthetic fluorapatite (Mariano 1988). Energy-dispersive X-ray analysis confirmed that these green luminescent crystals are apatite. This mineral is found in abundance within a quartz-plagioclase mica-schist inclusion sampled at 824 m and in small amounts in a large granitic inclusion from a depth of 888 m. Groundmass is sometimes seen to protrude into the fluidal-textured melt fragments within these samples. This could be a primary fluidal feature or the result of local thinning of a particle and grinding into groundmass during thin section preparation. Groundmass is also found as fills within round or ovoid blebs in melt fragments (Fig. 13d). Irregular calcite blebs, usually with bright orange luminescence, are commonly found dispersed throughout melt fragments.

Because unit 4 is practically devoid of calcite, cathodoluminescence features for samples from this unit are subdued. Rare disseminated calcite crystals were only observed along a 6 mm-wide shear zone, suggesting migration of carbonate-bearing fluids along such deformation zones. The dark, opaque, possibly hydrocarbon-bearing veins that are commonly found within this unit lack any luminescence.

Various cathodoluminescence features and textures were observed within unit 5, which has the highest carbonate content of all impactite units. Sub-angular to sub-rounded melt fragments are typically found suspended in the carbonate groundmass. The groundmass contains numerous non-luminescent, euhedral dolomite crystals (Figs. 13e and 13f).

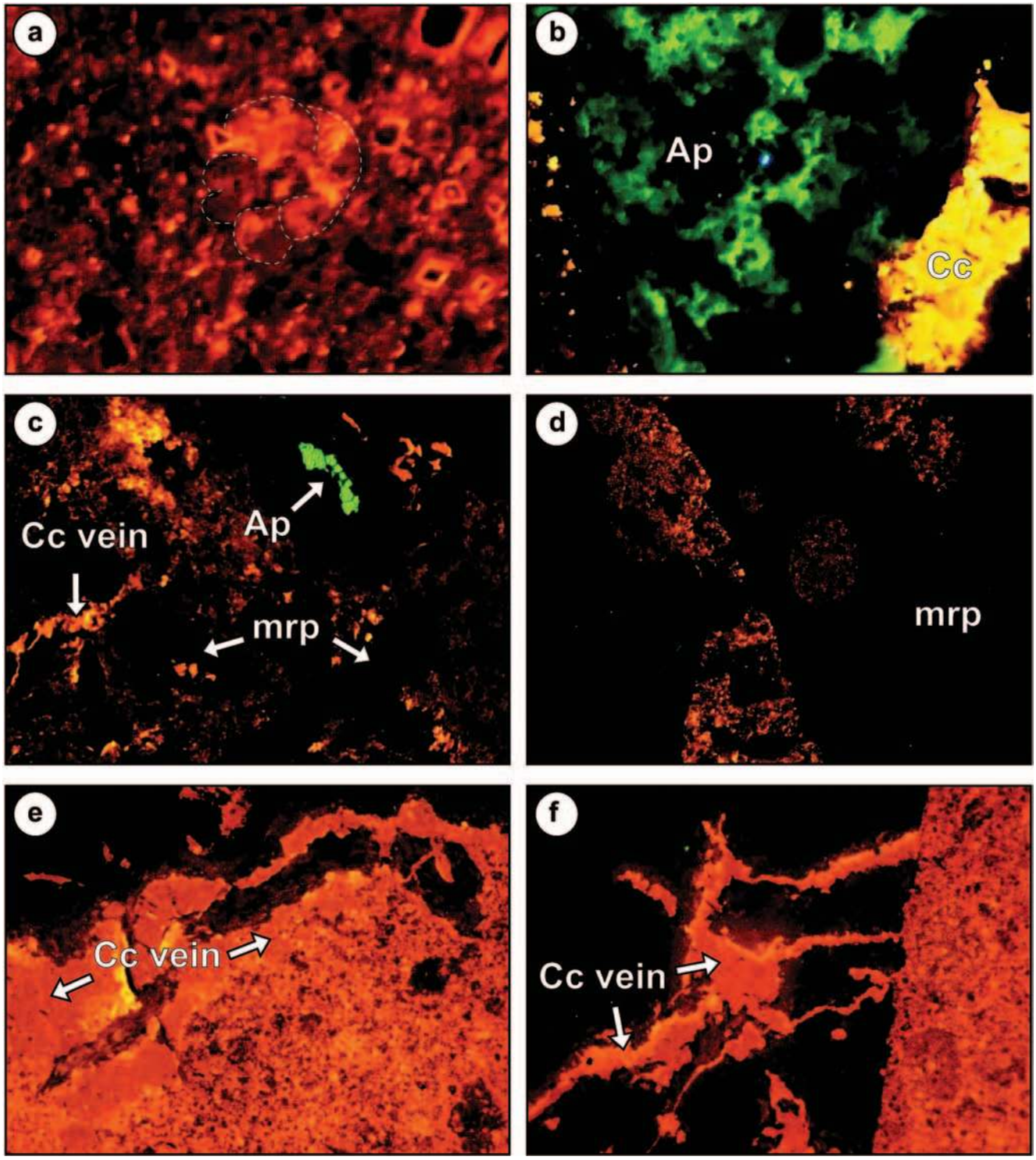

Fig. 13. Various cathodoluminescence photomicrographs of Yax-1 impactites: a) foraminifera bearing Tertiary limestone with oscillatory zoned calcite/dolomite rhombohedra; image width = 0.5 mm, sample depth = 791.71 m; b) green luminescent (melted apatite, Ap), and patchy texture within melt rock fragment; image width = 4 mm, sample depth = 821.39 m; c) mixed carbonate-silica groundmass with angular melt rock particles (mrp, no luminescence) showing well-preserved, fractured, green luminescent apatite (Ap) crystal; note the high luminosity of secondary carbonate veining; image width = 4 mm, sample depth = 822.90 m; d) vesicle in melt rock fragment, filled with mixed carbonate/altered glass groundmass material; image width = 2 mm, sample depth = 825.43 m; e) melt rock fragment with lining of high luminescent secondary calcite (Cc) vein (arrow); image width = 4 mm, depth = 886.79 m; f) melt rock fragment cross-cut by carbonate vein. Note the vein does not cross-cut the groundmass, indicating that it is younger; image width = 4 mm, sample depth = 886.79 m.

SEM-EDS analysis confirmed that the groundmass is rich in dolomite (Fig. 8d). Fine-grained carbonate veins with relatively high luminescence compared to the nearby groundmass are found lining melt fragments (Fig. 13e). Similar veins were noted in units 1 to 3. Pure calcite veins also cut silicate melt particles (Fig. 13f) but do not seem to continue into the surrounding groundmass.

DISCUSSION

The petrographic observations on the 100 m-thick impactite interval intersected in the Yax-1 borehole are discussed with respect to the following key issues: 1) the stratigraphic relationship with other boreholes; 2) the variation of petrographic features found throughout the impactite sequence; 3) the chemical composition of melt fragments; 4) the nature of the groundmass of the five units; 5) the implications for the emplacement of the various impactite units; and 6) the classification of the impactites.

Stratigraphic Relationship with Other Boreholes

When compared to previous drilling, the 100 m-thick impactite horizon of Yax-1 is much thinner than the intervals of impact breccia of 470 to 930 m thickness in the C1, S1, and Y6 drill cores (Ward et al. 1995; Sharpton et al. 1996; Stöffler et al. 2003b). Unfortunately, no seismic profiles were obtained for the Yax-1 site before drilling. Cretaceous rocks intersected by the boreholes toward the center of the impact crater, but still near Yax-1, occur at a much lower stratigraphic level (Fig. 2). The Y6 borehole was terminated in evaporitic rocks, i.e., dolomite and anhydrite, at a depth of 1630 m, whereas the C1 and S1 boreholes ended in melt rocks and breccias at 1581 m and ~1530 m, respectively (Ward et al. 1995; Sharpton et al. 1996; Stöffler et al. 2003b). Farther away from the center of the impact crater, the T1 borehole also intersected Cretaceous rocks at a shallower depth, i.e., ~900 m. The relative position of the Cretaceous rocks in the Yax-1 borehole is thought to be the result of slumping around the crater periphery, an area that is characterized by a prominent gravity low (Ebbing et al. 2001). With respect to the correlation of impactites from other boreholes, i.e., the Y6 borehole, we correlate our units 1 to 3 with the units 1 to 3 of Claeys et al. (2003). However, units 4 and 5 from the Yax-1 borehole do not seem to have equivalent subunits according to the observations of Claeys et al. (2003). A lower melt layer is suggested to occur below unit 3 in the Y6 borehole.

Features Common to the Entire Impactite Sequence

Before discussing the intrinsic details that characterize each unit, it is important to keep in mind that some features have been found that are typical for the entire impactite sequence. Units 2, 3, and 5 all contain melt fragments suspended in a groundmass, while unit 1 is composed of mostly self-supported melt rock and lithic fragments. Unit 4 has undergone in situ brecciation. Melt fragments are typically found as fluidal-textured, irregularly formed blebs or angular, shard-like particles. Lithic clasts are found throughout the entire sequence at relatively lower proportions than those of melt fragments (Table 3).

Some microscopic features are ubiquitous. Irregularly shaped carbonate blebs in silicate melt fragments can be alternatively interpreted as the result of immiscibility of a carbonate melt in silicate melt or as secondary carbonate-filled vesicles. They are common in melt particles of all units. Shock metamorphic features in lithic or mineral fragments, such as ballenquartz and quartz grains with PDFs, are also ubiquitous. Our statistics of shock-metamorphosed clasts do not indicate a substantial change of shocked mineral clast content or average shock degree with core depth/unit; however, a greater average number of PDFs in quartz grains is observed toward unit 5 (cf., Table 3). Unit 4 has by far more checkerboard feldspar than all other units. For such incipient melting to occur, shock pressures must have been in excess of 45 GPa, with post-shock temperatures between 900 and 1300 °C (Stöffler 1974; Bischoff and Stöffler 1984).

Clast compositions suggest that the lithic and mineral clast content of these impactites involved material from the upper carbonate platform and the underlying Pan-African basement. Lithic clasts are observed throughout the impactites. Inclusions that originate from the crystalline basement comprise primarily granitoid-derived fragments, schist and metapelite, quartzite, and rare amphibolite. Lithic inclusions that originate from the pre-impact sedimentary column comprise limestone, dolostone, fossiliferous limestone, calcareous sandstones, and quartzites. Anhydrite, which has been reported in abundance within the Cretaceous rocks of the Chicxulub structure (Ward et al. 1995; Dressler et al. 2003a) and as clasts in other impactite drill core intersections (Urrutia-Fucugauchi et al. 1996; Sharpton et al. 1999), only occurs in very small quantities (<1.5 vol%) throughout the Yax-1 sequence. The lithic and mineral clasts observed range from unshocked and weakly shocked material likely derived from the edge of the transient cavity to stronger shocked and, particularly, much melted material from closer to the point of impact. Unit 4 appears to be a brecciated impact melt rock that is interpreted to originate from melting of primarily crystalline basement. Our point count analysis reveals that only secondary carbonate occurs within this interval. Unit 4 comprises a massive melt rock unit and, as such, must have originated from a different region of the impact crater than units 1 to 3. Units 1 and 5 contain foraminifera fossils that could have originated from outside the transient cavity. They are essentially undeformed.

Secondary carbonate veins are observed throughout the impactite interval and indicate pervasive hydrothermal

overprint on the entire breccia sequence. However, there are distinctly more fractures with authigenic carbonate fill in units 2 and 3, between depths of 823 and 861 m, than in the other units.

Characteristics of the Overlying Reworked Interval

The upper reworked and suevitic material-bearing sedimentary interval between depths of 793 and 795 m contains several lenses (0.5–1.5 cm thick) of green, altered, suevitic material (similar to the underlying upper suevite) that is intercalated with grayish-white carbonate-rich rock. Distinct cross-lamination/bedding planes and rare drop stones of suevitic material are found within these sedimentary rocks. The cross-beds all have the same attitude (orientation) and, thus, indicate that the current followed a similar direction throughout deposition of this interval. The cross-beds typically appear as straight-crested, small-scale ripples and have a relatively high angle of repose that indicates good sedimentation rates with respect to ripple migration (Allan 1972). Because suevitic material is incorporated into the ripples, we suggest that the underlying impactite deposit was unconsolidated and, thus, easily reworked at the time of deposition of these sediments. However, the presence of rare suevite drop stones ("pebbles") indicates that some of the suevite was sufficiently lithified to be transported by current without disaggregation. These observations are more consistent with the suggestions of a tsunami/high-energy current (Goto et al. 2003) origin for this interval than with normal sedimentation (Keller et al. 2003b; Stinnesbeck et al. 2003). Apparently, the reworking of suevitic material took place immediately after cratering, i.e., after emplacement of the crater fill.

Unit 1: Several petrographic features are distinct to unit 1. Most strikingly, the average grain size of the fragmental lithic or melt material in this unit is much smaller (Fig. 2a) than that for the impactite units below. The primarily clast-supported character of this interval is also characteristic. The rocks, to a depth of 808 m, are very friable and poorly consolidated. Melt fragments are subrounded, without complex fluidal or angular morphologies that are typically observed in the lower units. A poor, but distinct, grading occurs from the top to the bottom of this unit. Overall, these features indicate progressive sorting with stratigraphic height, as also suggested by Dressler et al. (2003a, b), Kring et al. (2003a), and Stöffler et al. (2003a). Laminations were also reported by Dressler et al. (2003b).

The clast content is characterized by a distinctly greater proportion of microfossils and sedimentary clasts than observed in the lower units—with the exception of the lowermost unit 5 (Table 3). The superb preservation of these fossils (Fig. 3c), along with the greater proportion of carbonate clasts, could indicate detrital input from outside of the impact crater. The ratios of limestone to other clast proportions for samples of this unit are similar to those for the upper unit of the Y6 borehole (5 to 1), as observed by Claeys et al. (2003). Melt particles do not have microlites but strong perlitic fracturing (Fig. 3b), which can be interpreted as the result of relatively faster cooling of late fall-out into relatively cooler ocean water (perlitic fracturing indicates that the once glasses interacted with water; Ross and Smith 1955). Because the entire upper package between 795 and 823 m has similar features, including subrounded to subangular clast morphologies, the presence of carbonate clasts, foraminifera microfossils, and a clast-supported character, the two upper units, as defined by Dressler et al. (2003a), are here grouped together into unit 1. We suggest that these common characteristics far outweigh the differences reported by Dressler et al. (2003a) for the intervals of 795–808 m and 808–823 m, specifically the unconsolidated and fine-grained nature of the uppermost (795–808 m) segment in contrast to the more coherent nature of the lower interval.

We propose that this upper interval has been reworked by high-energy sedimentary processes in the form of a turbulent back-surge of seawater into the impact basin. The influx of seawater would have been responsible for transport and deposition of unshocked detritus into the impactite material, as observed by foraminifera microfossils and the unusually high carbonate clast content. This interpretation relates to the turbulent reworking invoked for several proximal Chicxulub ejecta sites around the Caribbean Sea (Bourgeois et al. 1988; Smit et al. 1992, 1996; Smit 1999; Takayama et al. 2000; Tada et al. 2002; Goto et al. 2002; Claeys et al. 2003). The resurge process has been recognized at several impact craters formed in the shallow marine realm, i.e., the Lockne (Ormö and Miyamoto 2002), Kaluga (Masaitis 2002), and Wetumpka (King et al. 2002) impact craters.

Units 2 and 3: The variegated character of the melt particles of unit 3 compared to the uniform green color of melt fragments in unit 2 is the main characteristic that differentiates these two units (Figs. 2b and 2c). The fragment sizes and morphological features are similar. A progressive increase in melt fragment size is observed with depth and may indicate a primary sorting effect. Another observation made on unit 2 by Dressler et al. (2003a) indicated that the groundmass had a "chocolate-brown" color as it was retrieved from the borehole but that the color changed to medium gray upon the drying of the core. This temporary coloration was also used to determine the extent of this unit. Macroscopically, some of the melt particles reveal fluidal and undulating contacts with the host groundmass, which is indicative of a primary deposit or that it was, at least, not mechanically reworked like the unit above. Kring et al. (2003a) reported that unit 2 was, in part, clast-supported and showed an increase in matrix content, from 15 to 24 vol%, between 823 and 846 m. We report modal proportions of 3 to 25 vol% for matrix in this unit. Our modal data do not indicate whether or not there is, indeed, an increase in matrix proportion with depth. In agreement with Kring et al.

(2003a), we recognize that the melt fragment content in units 2 and 3 is high (between 50 and 80 vol%). It was also reported that the groundmass of this interval was most likely of secondary origin, as it comprises abundant alkali elements (Na and K) and well-defined carbonate crystals (Kring et al. 2003a). It is, thus, supposed that carbonate probably replaced a clastic matrix (Stöffler et al. 2003a). With respect to the emplacement mechanism of units 2 and 3, we favor fallout of primary ejecta from an impact-induced debris cloud/plume, as large and small melt particles display fluidal and undulating morphologies (Figs. 3b and 3c). We suggest that the uniform green color of unit 2 represents a hydrothermal overprint and that this material likely represents rocks, from which the reworked unit 1 material was derived.

Unit 4: Unit 4, between depths of 861–885 m, represents a massive, brecciated, green melt rock unit. Macroscopic observations indicate that brecciation occurred in situ, as fragments fit together like the parts of a jigsaw puzzle. The fractures between fragments appear to be filled by a dark opaque material that, under the microscope, is non-reflective and, thus, could represent hydrocarbons. The melt is locally extensively altered, and veins filled with acicular crystals (thought to have been chlorite, now totally converted to sepiolite) are found throughout, commonly in close association with the opaque veining. The heat derived from this melt rock unit is suggested to have thermally metamorphosed and dehydrated the overlying unit 3, preserving its variegated character. This metamorphism is also believed to have increased the grain size character of unit 3 groundmass, similar to the thermal effect on the so called "thermometamorphic breccia unit" observed in the Y6 borehole (Claeys et al. 2003).

Because this unit contains hardly any carbonate material, no carbonate inclusions or foraminifera, and numerous silicate mineral fragments and inclusions (see Table 3), it is suggested that it must represent an allogenic deposit formed entirely from siliceous, crystalline basement-derived material. Any carbonate observed in this unit is restricted to some secondary veins. As the Yax-1 borehole is thought to be located just outside (~10 km; Morgan et al. 1997) the limits of the now collapsed transient cavity, transport from the source region is constrained to approximately 10 to 60 km, which is the maximum radial distance to the crater center. As unit 4 represents the second unit to be deposited in the impactite interval, it must have been deposited relatively early during the impact process. We suggest that unit 4 could either be an isolated melt pod or an outer part of a greater, perhaps coherent, melt sheet (see also Kring et al. 2003b).

Unit 5: Unit 5, at the base of the impactite sequence, comprises a complex mixture of lithic and melt fragments suspended in a fine- to medium-grained, carbonate-dominated groundmass. The polymict nature of the unit and the high content of carbonate clasts indicate that extensive mixing occurred between a diversity of target rock types, including Cretaceous carbonate. The presence of foraminifera microfossils within carbonate fragments (Table 3) indicates complete melting, or dissociation of carbonates, was not achieved in this unit. This is in contrast to units 2 through 4, where no fossils or preserved carbonate inclusions were found. The stratigraphic position of unit 5 indicates that it was the first impactite deposited. Stöffler et al. (2003a) suggested that the rocks might have been emplaced as an initial ground-surge deposit. We agree with this interpretation because of the diverse lithic content and the high carbonate versus silicate content, likely derived from the excavation and mixing of carbonate rocks of the upper stratigraphy of the area around the transient cavity.

There is conflicting evidence regarding the hydrothermal or primary impact melt origin of the carbonate groundmass of this unit. Unequivocal evidence for hydrothermal activity is indicated by the growth of euhedral barite grains in vesicles and the presence of iron-oxide lined vugs. Nevertheless, in support of a primary impact melt origin, Kring et al. (2003a) pointed out that melt fragments in this unit are groundmass-supported. The groundmass appears to contain at least 12 vol% melt fragments and numerous monomineralic clasts (Fig. 8b). Microprobe analyses indicate that melt fragments in the groundmass have high wt% totals and, thus, are volatile-poor and relatively unaltered. Also, macroscopic textural observations indicate that fluidal contacts are locally preserved (Fig. 2f). In contrast, a secondary origin of the groundmass carbonate is favored by the lack of clear cross-cutting relationships between the groundmass and carbonate veining. No calcite crystals with quenched acicular radiating textures were observed that could indicate that this groundmass is a melt phase, as observed by Claeys et al. (2003). Carbonate veins are observed cutting through melt fragments and not the groundmass, suggesting that the veins could be older than the groundmass (Fig. 13f). In contrast, carbonate veins meandering around melt fragments indicate that these veins are younger than the groundmass (Fig. 13e). Because of this conflicting evidence, it is still too early, if not eventually impossible, to determine accurately the hydrothermal or impact melt origin of this groundmass.

Microprobe Analysis of Melt

The composition of many melt fragments from the entire impactite sequence was determined by electron microprobe spot and traverse analysis (Fig. 10). These results indicate that the melt particles are of extremely variable composition, both between fragments and between zones within individual fragments. This is in agreement with the studies of Sharpton et al. (1992), Kettrup et al. (2000), and Claeys et al. (2003) of melts from the Y6 and C1 cores. Based on composition, at

least three types of melt particles were identified: mafic, mafic-alkali element-rich, and alkali element-rich, the latter occurring in greater abundances. In contrast to Hecht et al. (2003a), we did not analyze any silica-dominated melt particles. The feldspathic component-rich melt fragments show variable degrees of hydration with a significant proportion of analyzed fragments still yielding high total wt% values that are interpreted as evidence for relative "freshness" (e.g., Fig. 10b). Some fragments are of unusually high CaO contents that coincide with high K_2O concentrations and, thus, yield non-stoichiometric normative feldspar compositions. The high K contents can be attributed to K-metasomatic overprint (e.g. Hecht et al. 2003b), primary mixing of plagioclase and alkali feldspars, or to the incorporation of lime from decomposed carbonates into siliceous melt rock particles. We have been able to observe that at least some of the melt analyses indicate the presence of unaltered mineral melts, as indicated, for example, by K-feldspar composition and stoichiometric plagioclase melts (e.g., albite). Many fragments, however, and especially all mafic melt particles, show variable degrees of alteration, in accordance with the pervasive interaction of fluid phases after deposition. Such alteration has been observed at several impact sites, notably at the Ries, Lonar, and Mistastin Craters, where the impact melt particles and glasses were converted to saponite and montmorillonite (e.g., Osinski 2003; Hagerty and Newsom 2003). Variable degrees of K-metasomatism are also indicated by the K contents of mafic particles (Fig. 11c), alkali element-rich fragments (Fig. 12a), and melt phases in some checkerboard plagioclase grains (Fig. 12c). The melt fragment analyses indicate that the melt phases did not undergo extensive homogenization and that, instead, mineral or mineral combination melts form schlieren within the variegated melt fragments.

Classification of the Yax-1 Impactite Interval

According to the proposed impactite classification scheme of Stöffler and Grieve (1994), the entire sequence intersected in the Yax-1 section can be defined as suevitic breccia and impact melt rock. Suevite is defined as containing melt particles suspended within a matrix dominated by clastic material (e.g., Stöffler 1974; Dressler and Reimold 2001). Macroscopic observations alone would suggest that units 1 to 3 represent suevitic rocks. However, microscopy cannot resolve the exact nature of the groundmass of units 1 to 3. Our SEM investigations are generally in agreement with the features noted by Kring et al. (2003a), with the groundmass comprising calcite and alkali element-rich phases. It is difficult to support a total hydrothermal origin for this groundmass, as well-preserved monomineralic inclusions and small melt particles are quite abundant.

Unit 4 is an obvious impact melt rock, as it comprises a zone of now-altered melt with abundant microlites. Unit 5 contains melt particles and a minor component of lithic debris suspended in the carbonate-dominated groundmass; however, conflicting evidence concerning the nature of the groundmass (secondary or primary?) also prohibits accurate classification. If unit 5 contains a secondary carbonate groundmass that replaced or overprinted a primary lithic-plus-melt-fragment matrix, then the rock should be classified as a suevite (Stöffler et al. 2003a). If the groundmass, indeed, represents a carbonate melt, than the rock is basically an impact melt rock with a minor lithic clast content.

SUMMARY

The Yax-1 borehole, at a distance of ~60 km from the crater center, intersected an about 100 m-thick section of impactites. Similar to the impactite sections in the boreholes located closer to the center of the impact structure (C1, S1, Y6, and T1 boreholes), large quantities of melt fragments with minor proportions of lithic or mineral inclusions were observed throughout the sequence. We subdivide the 100 m sequence into five units, based on the melt particles' morphology, size, color, and abundance. Microscopic shock deformation such as PDFs in quartz and ballenquartz occurs throughout the impactite interval, in addition to the presence of checkerboard feldspar, which is mainly in unit 4. The melt fragment compositions are highly variable, and they have undergone a substantial amount of alteration to phyllosilicate phases. All mafic melt particles are strongly hydrated in comparison to alkali element-Si-rich melt particles that, at least in part, still yield good analytical totals and, thus, presumably original compositions. Both alkaline and mafic melt fragments show evidence for a K-metasomatic event that affected the entire sequence of impactite.

The conflicting evidence observed does not allow resolving the impact melt or authigenic origin of the carbonate component in the groundmass of unit 5. This unresolved issue arises from the fact that alteration and hydrothermal processes have been pervasive throughout the impactite sequence and that textural observations, such as possible liquid immiscibility features that might be interpreted to indicate impact melting of carbonate, are not conclusive.

Dressler et al. (2003a) subdivided the impactite sequence into 6 units based on the variable proportions of glass, lithic fragments, and groundmass; in contrast, we prefer a five-fold subdivision. We argue that units 1 and 2 of Dressler et al. (2003a) belong to the same unit that records a distinct mode of origin but does not have a uniform preservation state. Our unit 1 (795–823 m) represents a reworked fallout deposit, units 2 (823–846 m) and 3 (846–861 m) represent a pristine fallout suevite deposit, unit 4 (861–885 m) represents an allogenic siliceous melt rock body, and unit 5 (885–895 m) could represent an early suevitic or impact melt deposit. Further work is needed to elucidate the still unresolved origin of the carbonate groundmass in some of the Yax-1 impactites.

Acknowledgments–We gratefully acknowledge the comprehensive financial support for this project from the Petroleum Research Fund (grant PRF # 37299-AC8) of the American Chemical Society. Our analytical work has been generously supported by the Director of the South African Council of Geosciences, Pretoria. C. Koeberl was supported by the Austrian Science Foundation (Y58-GEO). We are also grateful for the detailed reviews by T. Kenkmann and P. Claeys. This is University of the Witwatersrand Impact Cratering Research Group Contribution No. 77.

Editorial Handling—Dr. Dieter Stöffler

REFERENCES

Allan J. R. L. 1972. A theoretical and experimental study of climbing-ripple cross lamination, with a field application to the Uppsala esker. *Geographic Annals* 53A:157–187.

Ames D., Dressler B., Pope K. O., and Pilkington M. 2003. Chicxulub impact structure hydrothermal activity (abstract #07331). Geophysical Research Abstracts 5. CD-ROM.

Alvarez L. W., Alvarez W., Asaro F., and Michel H. V. 1980. Extra-terrestrial cause for the Cretaceous-Tertiary extinction. *Science* 208:1095–1108.

Alvarez W., Claeys P., and Kieffer S. W. 1995. Emplacement of K/T—Boundary shocked quartz from the Chicxulub crater. *Science* 269:930–935.

Argyle E., Cisowski S. M., Fuller M., Officer C. B., and Ekdale A. A. 1986. Cretaceous extinctions and wildfires. *Science* 234:261–263.

Bischoff A. and Stöffler D. 1984. Chemical and structural changes induced by thermal annealing of shocked feldspar inclusions in impact melt rocks from Lappajärvi crater, Finland. *Journal of Geophysical Research* 89:B645–B656.

Blum J. D., Chamberlain C. P., Hingston M. P., Koeberl C., Marin L. E., Schuraytz B. C., and Sharpton V. L. 1993. Isotopic comparison of K/T boundary impact glass with melt rock from the Chicxulub and Manson impact structures. *Nature* 364:325–327.

Bohor B. F. 1990. Shocked quartz and more; Impact signatures in Cretaceous/Tertiary boundary clays. In *Global catastrophes in Earth history,* edited by Sharpton V. L. and Ward P. D. Special Paper 247. Boulder: Geological Society of America. pp. 335–342.

Bostwick J. A. and Kyte F. T. 1996. The size and abundance of shocked quartz in Cretaceous-Tertiary boundary sediments from the Pacific basin. In *The Cretaceous-Tertiary event and other catastrophes in Earth history,* edited by Ryder G., Fastovsky D. and Gartner S. Special Paper 307. Boulder: Geological Society of America. pp. 403–415.

Bourgeois J., Hansen T. A., Wiberg., P.L., and Kauffman E. G. 1988. A tsunami deposit at the Cretaceous-Tertiary boundary in Texas. *Science* 241:567–570.

Buseck P. R. 2002. Geological fullerenes: Review and analysis. *Earth and Planetary Science Letters* 203:781–792.

Chaussidon M., Sigurdsson H., and Métrich N. 1996. Sulfur and boron isotope study of high-Ca impact glass from the K/T boundary: Constraints on source rocks. In *The Cretaceous-Tertiary event and other catastrophes in Earth history,* edited by Ryder G., Fastovsky D., and Gartner S. Special Paper 307. Boulder: Geological Society of America. pp. 253–262.

Cisowski S. M. 1990. The significance of magnetic spheroids and magnesioferrite occurring in K/T boundary sediments. In *Global catastrophes in Earth history,* edited by Sharpton V. L. and Ward P. D. Special Paper 247 Boulder: Geological Society of America. pp. 359–365.

Claeys P., Heuschkel S., Lounejeva-Baturina E., Sanchez-Rubio G., and Stöffler D. 2003. The suevite of drill hole Yucatán 6 in the Chicxulub impact crater. *Meteoritics & Planetary Science* 38: 1299–1317.

Deer W. A., Howie R. A., and Zussman J. 1996. *An introduction to the rock forming minerals,* 2nd edition. Essex: Longman Scientific and Technical. 696 p.

Dressler B. O. and Reimold W. U. 2001. Terrestrial impact melt rocks and glasses: *Earth Science Reviews* 56:205–284.

Dressler B. O., Sharpton V. L., Morgan J., Buffler R., Moran D., Smit J., Stöffler D., and Urrutia-Fucugauchi J. 2003a. Investigating a 65 Ma-old smoking gun: Deep drilling of the Chicxulub impact structure. *Eos* 84:125, 131.

Dressler B. O., Sharpton V. L. and Marin L. E. 2003b. Chicxulub Yax-1 impact breccias: Whence they come? (abstract #1259). 34th Lunar and Planetary Science Conference. CD-ROM.

Ebbing J., Janle P., Koulouris J., and Milkereit, B. 2001. 3D gravity modelling of the Chicxulub impact structure. *Planetary and Space Science* 49:599–609.

Eskola P. 1939. *Die Entstehung der Gesteine.* Berlin: Julius Springer.

Evans N. J., Ahrens T. J., and Gregoire D. C. 1995. Fractionation of ruthenium from iridium at the Cretaceous-Tertiary boundary. *Earth and Planetary Sciences Letters* 134:141–153.

Freyssinet P. 2000. Geochemical mass balance and weathering rates of ultramafic schists in Amazonia. *Chemical Geology* 170:133–151.

Fuhrman M. L. and Lindsley D. H. 1988. Ternary-feldspar modeling and thermometry. *American Mineralogist* 73:201–215.

Gayraud J., Robin E., Rocchia R., and Froget L. 1996. Formation conditions of oxidized Ni-rich spinel and their relevance to the K/T boundary event. In *The Cretaceous-Tertiary event and other catastrophes in Earth history,* edited by Ryder G., Fastovsky D. and Gartner S. Special Paper 307. Boulder: Geological Society of America. pp. 424–443.

Gilmour I., Russell S. S., Arden J. W., Lee M. R., Franchi I. A., and Pillinger C. T. 1992. Terrestrial carbon and nitrogen isotopic ratios from Cretaceous-Tertiary boundary nanodiamonds. *Science* 258:1624–1626.

Goto K., Nakano Y., Tajika E., Tada R., Iturralde Vinent M. A., and Matsui T. 2002. Constraint on the depositional process of the K/T boundary proximal deep-sea deposit in northwestern Cuba based on shocked quartz distribution and its grain size (abstract). *Geological Society of America Abstracts with Programs* 34:239-10.

Goto K., Tada R., Bralower T. J., Tajika E., and Matsui T. 2003. Probability of marine invasion into the Chicxulub crater and consequent generation of large tsunamis (abstract #14413). Geophysical Research Abstracts 5. CD-ROM.

Grieve R. A. F. and Therriault A. M. 2000. Vredefort, Sudbury, Chicxulub: Three of a kind? *Annual Reviews in Earth and Planetary Science* 28:305–338.

Hagerty J. J. and Newsom H. E. 2003. Hydrothermal alteration at the Lonar Lake impact structure, India: Implications for impact cratering on Mars. *Meteoritics & Planetary Science* 38:365–381.

Hecht L., Kenkmann T., Schmitt R. T., Stöffler D., Tagle R., and Wittmann A. 2003a. Petrography, composition, shock metamorphism, and geology of the impact formations of the ICDP drill core Yax-1, Chicxulub crater, Mexico (abstract). 66th Annual Meteoritical Society Meeting.

Hecht L., Schmitt R. T., and Wittman A. 2003b. Hydrothermal alteration of the impactites at the ICDP drill site Yax-1 (Chicxulub crater) (abstract #1583). 34th Lunar and Planetary Science Conference. CD-ROM.

Heymann D., Chibante L. P. F., Brooks R. R., Woolbach W. S., and Smalley R. E. 1994. Fullerenes in the Cretaceous-Tertiary boundary layer. *Science* 256:645–647.

Heymann D., Chibante L. P. F., Brooks R. R., Woolbach W. S., Smit J., Korochantsev A., Nazarov M. A., and Smalley R. E. 1996. Fullerenes of possible wildfire origin. In *The Cretaceous-Tertiary event and other catastrophes in Earth history,* edited by Ryder G., Fastovsky D. and Gartner S. Special Paper 307. Boulder: Geological Society of America. pp. 453–464.

Hildebrand A. R., Penfield G. T., Kring D., Pilkington M., Camargo A., Jacobsen S. B., and Boynton W. 1991. Chicxulub crater: A possible Cretaceous-Tertiary boundary impact crater on the Yucatán peninsula, Mexico. *Geology* 19:867–871.

Hough R. M., Gilmour I., Pillinger C. T., Langenhorst F., and Montanari A. 1997. Diamonds from the iridium-rich K-T boundary layer at Arroyo el Mimbral, Tamaulipas, Mexico. *Geology* 25:1019–1022.

Hough R. M., Wright I. P., Sigurdsson H., Pillinger C. T., and Gilmour I. 1998. Carbon content and isotopic composition of K/T impact glasses from Haiti. *Geochimica et Cosmochimica Acta* 62:1285–1291.

Huffman A. R. and Reimold W. U. 1996. Experimental constraints on shock-induced microstructures in naturally deformed silicates. *Tectonophysics* 256:165–217.

Izett G. A. 1990. *The Cretaceous/Tertiary boundary interval, Raton Basin, Colorado and New Mexico, and its content of shock-metamorphosed minerals; Evidence relevant to the K-T boundary impact-extinction theory.* Special Paper 249. Boulder: Geological Society of America. 100 p.

Jarosewich E., Nelen J. A., and Norberg J. A. 1980. Reference standards for electron microprobe analysis. *Geostandards Newsletter* 4:43–47.

Kamo S. L. and Krogh T. E. 1995. Chicxulub crater source for shocked zircon crystals from the Cretaceous-Tertiary boundary layer, Saskatchewan: Evidence from new U-Pb data. *Geology* 23: 281–284.

Keller G., Stinnesbeck W., Adatte T., Stuben D. 2003a. Multiple impacts across the Cretaceous-Tertiary boundary. *Earth Science Reviews* 62:327–363.

Keller G., Adatte T., Stinnesbeck W., Steben D., Kramar U., and Harting M. 2003b. The K/T transition at the Yaxcopoil-1 drillhole (abstract #14415). Geophysical Research Abstracts 5. CD-ROM.

Keller G., Adatte T., Stinnesbeck W., Rebolledo-Vieyra M., Urrutia Fucugauchi J., Kramar U., and Stüben D. 2004. Chicxulub impact predates the K-T boundary mass extinction. *Proceedings of the National Academy of Sciences* 101:3753–3758.

Kenkmann T., Wittmann A., Scherler D., and Schmitt R. T. 2003. Deformation features of the Cretaceous units of the ICDP-Chicxulub drill core Yax-1 (abstract #1368). 34th Lunar and Planetary Science Conference. CD-ROM.

Kettrup B., Deutsch A., Ostermann M., and Agrinier P. 2000. Chicxulub impactites: Geochemical clues to the precursor rocks. *Meteoritics & Planetary Sciences* 35:1229–1238.

Kettrup B. and Deutsch A. 2003. Geochemical variability of the Yucatán basement: Constaints from crystalline clasts in Chicxulub impactites. *Meteoritics & Planetary Sciences* 38: 1079–1092.

King D. T., Jr., Neathery T. L., Petruny L. W., Koeberl C., and Hames W. E. 2002. Shallow-marine impact origin of the Wetumpka structure (Alabama, USA). *Earth and Planetary Science Letters* 202:541–549.

Koeberl C. 1993. Chicxulub crater, Yucatán: Tektites, impact glasses, and the geochemistry of target rocks and breccias. *Geology* 21: 211–214.

Koeberl C. and Sigurdsson H. 1992. Geochemistry of impact glasses from the K/T boundary in Haiti: Relation to smectites and new type of glass. *Geochimica et Cosmochimica Acta* 56: 2113–2129.

Koeberl C. and McLeod K. 2002. *Impacts and beyond.* Special Paper 356. Boulder: Geological Society of America. 749 p.

Koeberl C., Sharpton V. L., Schuraytz B. C., Shirey S. B., Blum J. D., and Marin L. E. 1994. Evidence for a meteoritic component in impact melt rock from the Chicxulub structure. *Geochimica et Cosmochimica Acta* 58:1679–1684.

Kring D. A. and Boynton W. V. 1992. Petrogenesis of an augite-bearing melt rock in the Chicxulub structure and its relationship to K/T impact spherules in Haiti. *Nature* 358:141–144.

Kring D. A. and Durda D. D. 2001. The distribution of wildfires ignited by high-energy ejecta from the Chicxulub impact event (abstract #1447). 32nd Lunar and Planetary Science Conference. CD-ROM.

Kring D. A., Hörz F., and Zurcher L. 2003a. Initial assessment of the excavation and deposition of impact lithologies exposed by the Chicxulub scientific drilling project, Yaxcopoil-1, Mexico (abstract #1641). 34th Lunar and Planetary Science Conference. CD-ROM.

Kring D. A., Zurcher L., and Hörz F. 2003b. Impact lithologies and post-impact hydrothermal alteration exposed by the Chicxulub scientific drilling project, Yaxcopoil, Mexico (abstract #4112). 3rd International Conference on Large Meteoritic Impacts. CD-ROM.

Krogh T. E., Kamo S. L., Sharpton V. L., Marin L. E., and Hildebrand A. R. 1993. U-Pb ages of single shocked zircons linking distal K/T ejecta to the Chicxulub crater. *Nature* 366:731–734.

Kyte F. T., Zhou Z., and Wasson J.T. 1980. Siderophile-enriched sediments from the Cretaceous-Tertiary boundary. *Nature* 288: 651–656.

Kyte F. T. and Bostwick J. A. 1995. Magnesioferrite spinel in Cretaceous/Tertiary boundary sediments of the Pacific basin: Remnant of hot, early ejecta from the Chicxulub impact? *Earth and Planetary Science Letters* 132:113–127.

Langenhorst F. and Deutsch A. 1994. Shock experiments on pre-heated α- and β- quartz: I. Optical and density data. *Earth and Planetary Science Letters* 128:683–698.

Mariano A. N. 1988. Some further geological applications of cathodoluminescence. In *Cathodoluminescence of geological materials,* edited by Marshall D. J. Winchester: Allen and Unwin Inc. pp. 94–123.

Marshall D. J. 1988. *Cathodoluminescence of geological materials.* Winchester: Allen and Unwin Inc. 146 p.

Masaitis V. L. 2002. The middle Devonian Kaluga impact crater (Russia): New interpretation of marine setting. *Deep-Sea Research II* 49:1157–1169.

Meldin W. L. 1963. Emission centers in thermoluminescent calcite, dolomite, magnesite, aragonite, and anhydrite. *Journal of the Optical Society of America* 53:1276–1285.

Meyerhoff A. A., Lyons J. B., and Officer C. B. 1994. Chicxulub structure: A volcanic sequence of Late Cretaceous age. *Geology* 22:3–4.

Morgan J., Warner M., The Chicxulub Working Group, Brittan J., Buffler R., Camargo A., Christeson G., Denton P., Hildebrand A., Hobbs R., MacIntyre H., MacKenzie G., Maguire P., Marin L., Nakamura Y., Pilkington M., Sharpton V. L., Snyder D., Suarez G., and Trejo A. 1997. Size and morphology of the Chicxulub impact crater. *Nature* 390:472–476.

Morgan J. V., Warner M. R., Collins G. S., Melosh H. J., and Christeson G. L. 2000. Peak-ring formation in large impact craters: Geophysical constraints from Chicxulub. *Earth and Planetary Science Letters* 183:347–354.

Morgan J., Warner M., and Grieve R. A. F. 2002. Geophysical constraints on the size and structure of the Chicxulub impact crater. In *Catastrophic events and mass extinctions: Impacts and beyond,* edited by Koeberl C. and MacLeod K. G. Special Paper 356. Boulder: Geological Society of America. pp. 39–46.

Ormö J. and Miyamoto H. 2002. Computer modelling of the water resurge at a marine impact: The Lockne crater, Sweden. *Deep-Sea Research II* 49:983–994.

Orth C. J., Gilmore S., Knight J. D., Pillmore C. L., Tschudy R. H., and Fasset J. E. 1981. An iridium abundance anomaly at the palynological Cretaceous-Tertiary boundary in northern New Mexico. *Science* 214:1341–1343.

Osinski G. R. 2003. Impact glasses in fallout suevites from the Ries impact structure, Germany: An analytical SEM study. *Meteoritics & Planetary Science* 38:1641–-1667.

Oskarsson N., Helgason O., and Sigurdsson H. 1996. Oxidation state of iron in tektite glasses from the Cretaceous/Tertiary boundary. In *The Cretaceous-Tertiary event and other catastrophes in Earth history,* edited by Ryder G., Fastovsky D., and Gartner S. Special Paper 307. Boulder: Geological Society of America. pp. 445–452.

Owen M. R., Anders M. H., Barber A. A., Condon P. D., and Haughton M. G. 1990. A closer look at cathodoluminescence of shocked quartz at the K/T boundary. In *Global catastrophes in Earth history,* edited by Sharpton V. L. and Ward P. D. Special Paper 247. Boulder: Geological Society of America. pp. 343–347.

Persaud P. and Sharpton V. L. 1998. Correlation of well data for the Chicxulub impact structure using gravity and magnetic anomalies. (abstract #1876). 29th Lunar and Planetary Science Conference. CD-ROM.

Penfield G. T. and Camargo Z. A. 1981 Definition of a major igneous zone in the central Yucatán platform with aeromagnetics and gravity (abstract). 51st Annual International Meeting of the Society of Exploration Geophysicists. p. 37.

Pope K. O., Baines K. H., Ocampo A. C., and Ivanov B. A. 1994. Impact winter and the Cretaceous/Tertiary extinctions: Results of a Chicxulub asteroid impact model. *Earth and Planetary Science Letters* 128:719–725.

Premo W. E. and Izett G. A. 1992. Isotopic signature of black tektites from the K-T boundary on Haiti—Implications for the age and type of source material. *Meteoritics* 27:413–424.

Righi D. and Meunier A. 1995. Origin of clays by rock weathering and soil formation. In *Origin and mineralogy of clays,* edited by Velde B. Berlin: Springer-Verlag. pp. 43–161.

Ross C. S. and Smith R. L. 1955. Water and other volatiles in volcanic glass. *American Mineralogist* 40:1071–1089.

Ryder G., Fastovsky D., and Gartner S. 1996. *The Cretaceous-Tertiary event and other catastrophes in Earth history.* Special Paper 307. Boulder: Geological Society of America. 580 p.

Schmitz B. 1988. Origin of microlayering in world wide distributed Ir-rich marine Cretaceous-Tertiary boundary clays. *Geology* 16: 1068–1072.

Schuraytz B. C., Sharpton V. L., and Marin L. E. 1994. Petrology of impact-melt-rocks at the Chicxulub multiring basin, Yucatán, Mexico. *Geology* 22:868–872.

Sharpton V. L. and Ward P. D. 1990. *Global catastrophes in Earth history; An interdisciplinary conference on impacts, volcanism, and mass mortality.* Special Paper 247. Boulder: Geological Society of America. 631 p.

Sharpton V. L., Dalrymple G. B., Marin L. E., Ryder G., Schuraytz B. G., and Urrutia-Fucugauchi J. 1992. New links between the Chicxulub impact structure and the Cretaceous/Tertiary boundary. *Nature* 359:819–821.

Sharpton V. L., Burke K., Camargo-Zanoguera A., Hall S. A., Scott Lee D., Marin L. E., Suárez-Reynoso G., Quezada-Muñeton J. M., Spudis P. D., Urrutia-Fucugauchi J. 1993. Chicxulub multiring impact basin: Size and other characteristics derived from gravity analysis. *Science* 261:1564–1567.

Sharpton V. L., Marin L. E., Carney J. L., Lee S., Ryder G., Schuraytz B. C., Sikora P., and Spudis P. D. 1996. A model of the Chicxulub impact basin based on evaluation of geophysical data and drill core samples. In *The Cretaceous-Tertiary event and other catastrophes in Earth history,* edited by Ryder G., Fastovsky D., and Gartner S. Special Paper 307. Boulder: Geological Society of America. pp. 55–74.

Sharpton V. L., Corrigan C. M., Marin L. E., Urrutia-Fucugauchi J., and Vogel T. A. 1999. Characterization of impact breccias from the Chicxulub impact basin: Implications for excavation and ejecta emplacement (abstract #1515). 30th Lunar and Planetary Science Conference. CD-ROM.

Sharpton V. L. 2000. Exploring the Chicxulub impact basin through scientific drill-coring: Historical perspective and current plans. In *International conference on catastrophic events and mass extinction: Impacts and beyond.* Contribution No. 1053. Houston: Lunar and Planetary Institute.

Sigurdsson H., D'Hondt S., Arthur M. A., Bralower T. J., Zachos J. C., Fossen van M., and Channell J. E. T. 1991 Glass from the Cretaceous/Tertiary boundary in Haiti. *Nature* 349:482–487.

Smit J. 1999. The global stratigraphy of the Cretaceous-Tertiary boundary impact ejecta. *Annual Reviews in Earth and Planetary Sciences* 27:75–113.

Smit J. and Hertogen J. 1980. An extraterrestrial event at the Cretaceous-Tertiary boundary. *Nature* 285:198–200.

Smit J., Montanari A., Swinburne N. H. M., Alvarez W., Hildebrand A. R., Margolis S. V., Clayes P., Lowrie W., and Asaro F. 1992. Tektite-bearing, deep-water clastic unit at the Cretaceous-Tertiary boundary in northeastern Mexico. *Geology* 20:99–103.

Smit J., Roep B., Alvarez W., Montanari A., Claeys P., Grajales-Nishimura J. M., and Bermudez J. 1996. Coarse-grained, clastic sandstone comlex at the K/T boundary around the Gulf of Mexico: Deposition by tsunami waves induced by the Chicxulub impact? In *The Cretaceous-Tertiary events and other catastrophes in Earth history,* edited by Ryder G., Fastovsky D., and Gartner S. Special paper 307. Boulder: Geological Society of Americ. pp. 151–182.

Stinnesbeck W., Keller G., Adatte T., Harting M., Kramar U., and Stüben D. 2003. Yucatán subsurface stratigraphy based on the Yaxcopoil-1 drillhole (abstract #10868). Geophysical Research Abstracts 5. CD-ROM.

Stöffler D. 1974. Deformation and transformation of rock forming minerals by natural and experimental shock processes: II. Physical properties of shocked minerals. *Fortschritte der Mineralogie* 51:443–458.

Stöffler D. and Grieve R. A. F. 1994. Classification and nomenclature of impact metamorphic rocks: A proposal to the IUGS subcommission on the systematics of metamorphic rocks (abstract #1347). 25th Lunar and Planetary Science Conference. CD-ROM.

Stöffler D., Hecht L., Kenkmann T., Schmitt R. T., and Wittmann A. 2003a. Properties, classification, and genetic interpretation of the allochthonous impact formation of the ICDP Chicxulub drill core Yax-1 (abstract #1553). 34th Lunar and Planetary Science Conference. CD-ROM.

Stöffler D., Hecht L., Ivanov B. A., Kenkmann T., Salge T., Schmitt R. T., Schönian F., Tagle R., and Wittman A. 2003b. Characterisitcs of the multi-ring impact basin of Chicxulub, Mexico, as derived from drill core data and numerical modeling (abstract #5241). 66th Annual Meeting of the Meteoritical Society. CD-ROM.

Swisher C. C., III, Nishimura G., Montanari A., Margolis S. V.,

Claeys P., Alvarez W., Renne P., Cedillo-Pardo E., Maurasse F. J. -M. R., Curtis G. H., Smit J., and McWilliams M. O. 1992. Coeval $^{40}Ar/^{39}Ar$ ages of 65.0 million years ago from Chicxulub crater melt rock and Cretaceous-Tertiary boundary tektites. *Science* 257:954–958.

Tada R., Nakano Y., Iturralde-Vinent M. A., Yamamoto S., Kamata T., Tajika E., Toyoda K., Kiyokawa S., Garcia Delgado D., Oji T., Goto K., Takayama H., Rojas-Consuegra R., and Matsui T. 2002. Complex tsunami waves suggested by the Cretaceous-Tertiary boundary deposit at the Moncada section, western Cuba. In *Catastrophic events and mass extinctions: impacts and beyond,* edited by Koeberl C. and MacLeod K. G. Special Paper 356. Boulder: Geological Society of America. pp. 109–123.

Takayama H., Tada R., Matsui T., Irralde-Vinent M. A., Oji T., Tajika E., Kiyokawa S., Garcia D., Okada H., Hasegawa T., and Toyodo K. 2000. Origin of the Penalver formation in northwestern Cuba and its relation to the K/T boundary impact event. *Sedimentary Geology* 135:195–320.

Tuchscherer M. G., Reimold W. U., Gibson R. L., and Keoberl C. 2003. Petrographic observations and classification: Impactites from the Yaxcopoil-1 borehole, Chicxulub impact structure, Yucatán peninsula, Mexico (abstract #1310). 34th Lunar and Planetary Science Conference. CD-ROM.

Tuchscherer M. G., Reimold W. U., Koeberl C., and Gibson R. L. 2004. Major and trace element characteristics of impactites from the Yaxcopoil-1 borehole, Chicxulub structure, Mexico. *Meteoritics & Planetary Science*. This issue.

Urrutia-Fucugauchi J., Marin L., and Trejo-Garcia A. 1996. UNAM Scientific drilling program of Chicxulub impact structure—Evidence for a 300 kilometer crater diameter. *Geophysical Research Letters* 23:1565–1568.

Ward W. C., Keller G., Stinnesbeck W., and Adatte T. 1995. Yucatán subsurface stratigraphy: Implications and constraints for the Chicxulub impact. *Geology* 23:873–876.

Warren P. H., Claeys P. H., and Cedillo-Pardo E. 1996. Mega-impact melt petrology (Chicxulub, Sudbury, and the Moon): Effects of scale and other factors on potential for fractional crystallization and development of cumulates. In *The Cretaceous-Tertiary event and other catastrophes in Earth history,* edited by Ryder G., Fastovsky D. and Gartner S. Special Paper 307. Boulder: Geological Society of America. pp. 105–124.

Whitehead. 2004. Earth impact database. PASSC. University of New Brunswick. http://www.unb.ca/passc/ImpactDatabase/images.

Wolbach W. S., Lewis R. S., and Anders E. 1985. Cretaceous extinctions: Evidence for wild fires and search for meteoritic material. *Science* 230:167–170.

Wolbach W. S., Anders E., and Nazarov M. A. 1990. Fires at the K/T boundary: Carbon at the Sumbar, Turkmenia, site. *Geochimica et Cosmochimica Acta* 54:1133–1146.

Zurcher L. and Kring D. A. 2003. Preliminary results on the post-impact hydrothermal alteration in the Yaxcopoil-1 hole, Chicxulub impact structure, Mexico (abstract #1735). 34th Lunar and Planetary Science Conference. CD-ROM.